



University of
Stavanger

Faculty of Science and Technology

MASTER'S THESIS

Study program/ Specialization: Petroleum technology/ Reservoir engineering	Spring semester, 2011 Open
Writer: Ann Helen Kvæstad (Writer's signature)
Faculty supervisor: Svein Skjæveland External supervisor(s): Ingebret Fjelde	
Title of thesis: CO ₂ -foaming agent retention in fractured chalk models: Experiments and simulations	
Credits (ECTS): 30	
Key words: Enhanced oil recovery CO ₂ -foam Chalk Surfactant Retention	Pages: 71 Stavanger, 14/06/2011 Date/year

Acknowledgement

First of all I would like to thank my supervisor Dr. Ingebret Fjelde. He has provided me with an interesting and challenging master thesis, and good guidance and advices during the writing of my thesis.

I would like to thank Dr. John Fabricius Zuta for excellent support and help with the experiments and simulations during my thesis, and for his thoughts on how to present the thesis.

I will also thank my faculty supervisor, Prof. Svein Skjæveland, for reading through my thesis and giving his thoughts on it.

I wish to thank my family, friends and especially Kim Rene for encouragement and support during my studies.

Ann Helen Kvæstad

Abstract

Injection of CO₂-gas can improve the oil recovery. In naturally fractured reservoirs such as chalk, injection of CO₂-gas can result in early gas breakthrough because the gas can use the fractures as pathways from the injector to the producer. The pressure, temperature and oil properties in the reservoir can also lead to an unfavorable mobility for the gas. This can lead to low total sweep efficiency for the process. One method to increase the total sweep efficiency in the fractured reservoir is to use CO₂-foam. Foam has a higher apparent viscosity compared with gas alone, and this can increase the resistance to flow, thus the CO₂-mobility can be decreased. Retention of the foaming agent in the reservoir can cause instability of the foam. This can lead to foam collapse and the process can become more expensive because of the extra foaming agent that has to be injected.

In this thesis the retention and transport of the foam forming agent in fractured chalk models have been investigated in experiments and mechanistic simulations. This was performed at 100 % water saturation ($S_w = 100\%$) or residual oil saturation after water flooding (S_{orw}). Different surface area of the core plugs were blocked and was not exposed to the foaming agent solution. The objective was to see how the different designs would affect the retention and transport. In the modeling studies a reservoir simulator, STARS, from Computer Modeling Group (CMG) was used.

Experimental results show that transport of the foaming agent would depend on the design of the fractured model. It was also seen that the rate of retention increased with increasing surface area exposed. In this thesis S_{orw} did not have a significant effect on the retention of the selected foaming agent in the fractured model. In the simulations the concentration of the foaming agent in the fracture vs. time for core plugs at 100 % water saturation with all surface area exposed was history-matched. The same data set was used to predict the concentration of the foaming agent in the fracture for the other designs at 100 % water saturation. Further work with the foaming agent used in this thesis should be performed.

Table of content

ACKNOWLEDGEMENT	2
ABSTRACT	3
TABLE OF CONTENT.....	4
NOMENCLATURE.....	6
1. INTRODUCTION	8
1.1 Enhanced oil recovery.....	8
1.2 Objective	9
2. THEORY.....	10
2.1 CO ₂ -injection	10
2.2 CO ₂ -foam injection.....	14
2.3 Foaming agent	18
3. EXPERIMENTS.....	21
3.1 Porous media	21
3.2 Chemicals and fluids	21
3.3 Preparation of core plugs with FW	22
3.4 Preparation of core plugs with stock tank oil.....	24
3.5 Static retention experiments; fractured chalk model	24
3.5.1 Preparation of fractured chalk model	24
3.5.2 Procedure for static experiments	26
3.6 Static adsorption experiment	27
3.7 Flow-through retention experiments	27
3.8 Analytical methods	28
3.8.1 Two-phase titration with Hyamine	28
3.8.2 Sulfate analysis.....	29
3.8.3 Lithium analysis.....	29
4. NUMERICAL SIMULATION	30
4.1 Introduction	30
4.2 Simulation setup	30
5. RESULTS.....	33

5.1	Experimental results from fractured model experiments	34
5.1.1	No surface area blocked	35
5.1.2	Lateral surface area blocked	36
5.1.3	Lateral surface area and top blocked	37
5.1.4	Lateral surface area and bottom blocked	38
5.1.5	Half the lateral surface area and bottom blocked	40
5.1.6	Summary of the experimental results	41
5.2	Static adsorption experiment	44
5.3	Flow-through retention experiments	46
5.4	Numerical simulation of the fractured model experiment	49
5.4.1	No surface area blocked	51
5.4.2	Lateral surface area blocked	52
5.4.3	Lateral surface area and top blocked	54
5.4.4	Lateral surface area and bottom blocked	55
5.4.5	Half the lateral surface area and bottom blocked	57
5.4.6	Summary of the simulated results	58
5.5	Simulated results from the core plug with lateral surface area blocked	58
5.6	Larger scale simulations	60
5.7	Comparison	61
6.	DISCUSSION	63
7.	CONCLUSIONS	66
	REFERENCES	67

Nomenclature

A	The adsorption of foaming agent at equilibrium
ADMAXT	Maximum adsorption capacity in the matrix
ADRT	Residual adsorption level
C	Concentration of foaming agent in effluent samples
C_0	Concentration of foaming agent initially
CMC	Critical micelle concentration
CMG	Computer Modeling Group
E	Total sweep efficiency
E_D	Microscopic efficiency
E_V	Macroscopic efficiency
EOR	Enhanced oil recovery
$[FA]_{\text{diluted}}$	The foaming agent concentration due to dilution
$[FA]_{\text{End}}$	Concentration of foaming agent at the end of the experiments
$[FA]_{\text{Initial}}$	Concentration of foaming agent initially
FW	Formation water
ICP	Inductive Coupled Plasma
IOS	Internal olefin sulfonate
k_{abs}	Absolute permeability
k_i	Effective permeability of phase i , $i = d, D$
k_{ri}	Relative permeability of phase i , $i = d, D$
$k_{ro}(S_{wi})$	End point permeability for oil at initial water saturation
$k_{rw}(S_{orw})$	End point permeability for water at residual oil saturation after water flooding
λ_i	Mobility of phase i , $i = d, D$
M	Mobility ratio
MB	Methylene blue
μ_i	Viscosity of phase i , $i = d, D$

PORFT	Accessible pore volume
PV	Pore volume
R	Concentration of foaming agent retained in chalk
RRFT	Residual resistance factor
RT	Room temperature
S_{or}	Residual oil saturation
S_{orw}	Residual oil saturation after water flooding
SW	Sea water
SWL	Sea water with lithium
S_w	Water saturation
S_{wi}	Initial water saturation
$V_{fracture}$	The volume of the artificial fracture
V_{PV}	The pore volume of the core plug
W_{FAS}	Weight of foaming agent solution
W_{FAS}^{eq}	The weight of the foaming agent solution at equilibrium
W_{PV}	The weight of the FW in the pore volume of the core plug
W_{rock}	Weight of the core plug
wt%	Weight percent

1. Introduction

1.1 Enhanced oil recovery

Oil recovery can be subdivided into three processes; primary-, secondary- and tertiary oil recovery (Green and Willhite 1998, Latil 1980, Orr et al. 1982). During the primary oil recovery, the production is a result of the naturally existing displacement energy in the reservoir. The secondary production starts when the primary production starts to decline. Secondary oil recovery includes pressure maintenance by water or gas. The last oil recovery process is the tertiary oil recovery. This is also called enhanced oil recovery (EOR). EOR is a process when a fluid or fluids of some type is injected into a reservoir. The fluids can be miscible or immiscible gases, chemicals, or thermal energy. An EOR process can be performed to displace additional oil when secondary- or primary oil recovery processes no longer are economical. These three stages do not have to happen chronologically, and all of the stages do not have to be done. During both secondary and EOR processes the natural energy present in the reservoir is supplemented to displace oil to production wells. Oil recovery is enhanced because of the interactions between the injected fluid and the reservoir rock/oil system which creates favorable conditions. The total sweep efficiency, E , is the product of the microscopic efficiency, E_D , and the macroscopic efficiency, E_V (Green and Willhite 1998);

$$E = E_D \cdot E_V. \tag{1}$$

E_V is the product of areal and vertical displacement efficiencies, and it is the displacement on volumetric scale. E_D is displacement on pore scale and it is therefore dependent on the residual oil saturation, S_{or} , and initial water saturation, S_{wi} , in the pores (Green and Willhite):

$$E_D = \frac{1-Sw_i - S_{or}}{1-Sw_i}. \quad (2)$$

In an EOR process the objective is to increase E in such a way that it approaches 1, and one way of doing this is to reduce S_{or} . This causes E_D to increase, thus there will be higher E . E_V can be improved by having a favorable mobility ratio between the injected fluid and the reservoir fluid (Green and Willhite 1998). The density of the fluids is also important as to how well the sweep efficiency is.

1.2 Objective

An EOR process that has been investigated is the use of CO₂-foam. This process can increase the total sweep efficiency in a reservoir (Zuta et al. 2010a). The concern with CO₂-foam is the retention of foaming agent in the reservoir. This can affect both the cost and the stability of the process. In this thesis the objective was to investigate the rate of foaming agent retention and transport in fractured models with different designs using both experimental and modeling studies. The different designs were formed by blocking different surface area on the core plug; the blocked surface area would then not be exposed to the foaming agent solution. The static retention experiment that was performed in this thesis was done in a fractured chalk model. To investigate the retention for the foaming agent a static adsorption experiment and a flow-through experiment was also performed. The simulation with a reservoir simulator, STARS, was done to simulate the fractured chalk model.

The next chapter, Theory, is a literature study with focus on CO₂-gas injection, CO₂-foam injection and foaming agent.

2. Theory

2.1 CO₂-injection

The gases that can be injected into oil reservoirs to enhance the oil recovery during an EOR process can be steam, CO₂, nitrogen or enriched hydrocarbons (Apaydin and Kovscek 2000). The mechanisms that makes CO₂-injection a promising EOR process is that it can reduce the oil viscosity, swell the oil, and there is a mass transfer between CO₂ and oil which can lead to miscible CO₂-flood (Holm and Josendal 1974). CO₂ can be used as an immiscible or a miscible displacing fluid (Asghari and Torabi 2008). The injection of CO₂ is miscible at high pressures and immiscible at low pressures. Depending on reservoir pressure, temperature and on the composition of the crude oil one of the processes can happen. If the process is miscible, it can lead to good microscopic sweep efficiency, i.e. low S_{or} .

At most reservoir pressures and temperatures many of the gases that are used for EOR processes have densities and viscosities that are much lower than the fluids in the reservoir (Panahi 2004). The density and viscosity is dependent on the temperature and the pressure in the reservoir. At low temperatures the density of CO₂-gas is usually higher than the reservoir oil, but the density can be equal to the density of the reservoir water. The density of the CO₂-gas can be lower than both reservoir fluids at high temperatures. At most reservoir conditions CO₂ is a dense liquid-like fluid (Chang and Grigg 1999). The viscosity of CO₂ is much lower than the viscosity of the reservoir fluids for most reservoir conditions, and this difference can lead to instability in the displacement front (Panahi 2004). The difference in viscosity causes a difference in mobility between displacing and displaced fluids, and this can lead to an unfavorable mobility ratio (M). The mobility of fluid phase i , λ_i , is defined as (Green and Willhite 1998):

$$\lambda_i = \frac{k_i}{\mu_i}. \quad (3)$$

The equation shows how λ_i is dependent on the viscosity (μ_i) and the effective permeability (k_i) of the fluid phase. The ratio between the mobilities of the displacing phase and the displaced phase, M , is defined as (Green and Willhite 1998):

$$M = \frac{\lambda_D}{\lambda_d} = \frac{k_{rD} \mu_d}{\mu_D k_{rd}}. \quad (4)$$

Where k_{rD} and k_{rd} is the relative permeability of the displacing and displaced phase respectively, and μ_D and μ_d is the viscosity of displacing and displaced phase respectively. If the value of M is 1 or lower, the displacement will be stable (Figure 2.1a), and if M is larger than 1, the displacement will be unstable (Figure 2.1b). In an unstable displacement, the total sweep efficiency can be low and there can be large areas that can be left unswept (see example in Figure 2.1 and 2.2).

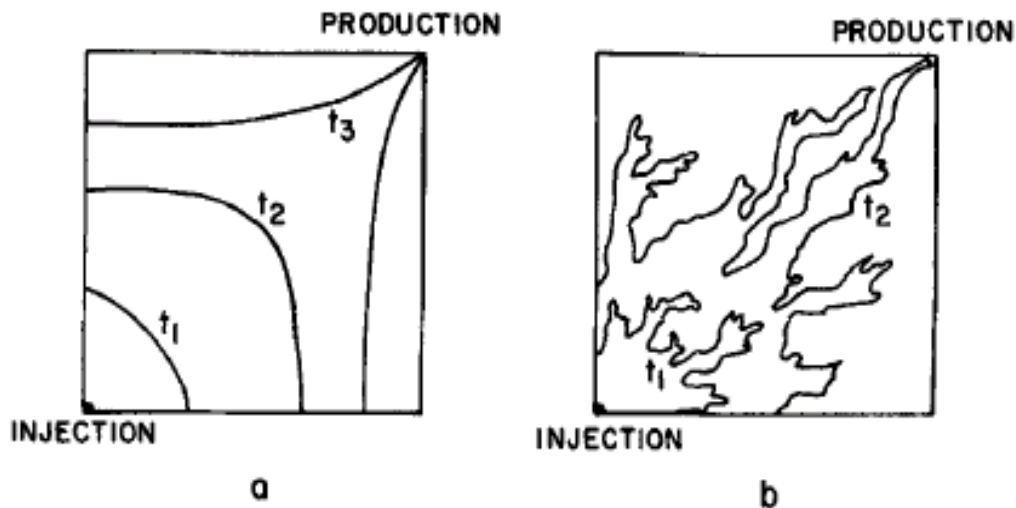


Figure 2.1: An example of area sweep efficiency; a) A stable displacement with a favorable mobility ratio; good macroscopic sweep, b) An unstable displacement with an unfavorable mobility ratio; poor macroscopic sweep (Orr et al. 1982).

The efficiency during injection of CO₂ can be low because of different reasons (Lee et al. 1991, Apaydin and Kavscek 2000):

- The reservoir can be heterogeneous and contain regions that have higher permeability than the other parts. In these regions the injected fluid can move faster to the producing wells than it can do in other parts of the reservoir (Figure 2.2a)
- The gas can rise to the top of the reservoir by gravity segregation (Figure 2.2b)
- The high mobility of CO₂ caused by the low viscosity can give a frontal instability that leads to viscous fingering, and that can give the flow a preferential route

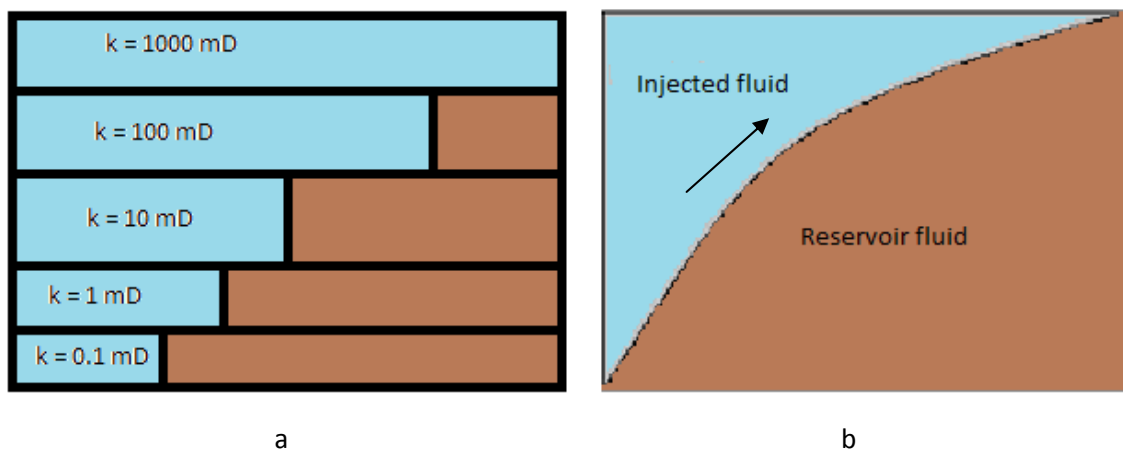


Figure 2.2: Vertical sweep efficiency. The blue area is the injected fluid, and the brown area is the reservoir fluid. Sketch a) is an example of how the injected fluid can flow if there are regions in the reservoir with different permeabilities. Figure b) is a sketch over gravity segregation.

These reasons can act alone or together, and they can cause bypassing of large amount of oil in the reservoirs (Lee et al. 1991). These points affect the macroscopic efficiency of the injection of CO₂ and they can result in an early breakthrough of the injected fluid. The first point can affect both the areal and vertical efficiency because of the regions with higher permeability. The vertical efficiency is mostly affected in the second point, and in the third point both areal and vertical efficiency can be affected. The low macroscopic efficiency affects the total sweep efficiency for the injection of CO₂-gas.

Carbonate reservoirs contain a considerable portion of the proven petroleum reserves in the world (Akbar et al. 2000). One type of carbonate reservoir is chalk. Chalk is a very pure form of calcium carbonate (Hardman 1982). The porosity in chalk can be quite high, 35 – 45 %, but the matrix permeability is low, 1 – 3 mD. Chalk reservoirs are naturally fractured, with different degree of fracturing. The chalk reservoirs need fractures for the oil to migrate into the reservoir, and the fractures makes it possible for oil production from the chalk. These fractures increase the effective permeability for the chalk.

The total oil recovery during CO₂-injection into fractured reservoirs is affected by several mechanisms; capillary and viscous forces, molecular diffusion, total pore compressibility, phase behavior, and gravity drainage (Darvish et al. 2006, Hoteit and Firoozabadi 2006). The mechanism which dominates depends on rock type, injection rate, fluid properties and rock-fluid interactions (Hoteit and Firoozabadi 2006).

The reason why the oil recovery often is low in fractured reservoirs is mainly because of early gas breakthrough through the fractures. The injected gas uses the fractures as a pathway directly from the injection wells to the production wells (Chakravarthy et al. 2006). An important parameter which can cause low oil recovery in reservoirs with fractures is the capillary pressure contrast of the fracture and the reservoir matrix (Firoozabadi and Markeset 1994, Dindoruk and Firoozabadi 1994).

To improve the sweep efficiency for CO₂-injection mobility-control can be used. Several methods have been considered to decrease the mobility of CO₂ (Chung 1991, Orr et al. 1982):

1. Disperse CO₂ in water with foaming agent to generate foam
2. Water-Alternating-Gas (WAG) process
3. Polymer-enhanced WAG process
4. Viscosifying the gas phase
5. In situ polymerization of soluble monomers in supercritical CO₂
6. Adding co-solvents in supercritical CO₂

2.2 CO₂-foam injection

To disperse CO₂ in water with a foaming agent was first patented by Bond and Holbrook in 1958. The definition of foam is that foam is a dispersion of gas in a liquid in such a way that the liquid phase is continuous and part of the gas phase is made discontinuous by thin liquid films called lamellae (Schramm and Wassmuth 1994, Falls et al. 1988, Kovsky et al. 1995). Most foam contains gas, liquid and a foaming agent (Schramm and Wassmuth 1994). Foams can be used for gas-mobility control in EOR, acid diversion in well stimulation, water shut-off and gas-blocking in water coning prevention and gas storage (Nguyen et al. 2000). Experiments and simulation results of CO₂-foam flooding in fractured chalk showed that CO₂-foam can give effective mobility control in fractured reservoirs (Zuta et al. 2010a). The study also showed that there was an increase in the effective viscosity of the CO₂-gas.

During foam flow in mobility control there can be a portion of bubbles trapped inside the porous media (Nguyen et al. 2000). The bubbles that are trapped are temporary blocking agents for gas flow. It is the lamellae that separate the foam into bubbles that block the pores and fractures in the reservoirs, and this causes the free flow of gas or other low-viscous fluids to be blocked (Lee et al. 1991). For the foam to be an effective displacing or blocking agent, the lamellae must be relatively stable (Apaydin and Kovsky 2000). The adsorption of the foaming agent at the gas/liquid interfaces stabilizes the lamellae (Schramm and Wassmuth 1994, Kovsky et al. 1995). These stabilizing forces are sensitive to foaming agent concentration and structure, temperature, pH, applied shear rate, volume ratio of water to oil, and to the ionic strength of the aqueous solution (Apaydin and Kovsky 2000, CMG Manual 2010.10).

Some of the factors that foam generation and coalescence is dependent on is foaming agent concentration, capillary pressure and gas flow rate (Chung 1991). There are three fundamental foam generation mechanisms; snap-off, lamellae division, and leave-behind, where snap-off is the dominant one (Kovsky and Radke 1994). Foam can be injected in three different ways (Lee et al. 1991, Shan and Rossen 2002, Ettinger and Radke 1992);

- Foam can be pre-formed before it is injected into the reservoir
- Co-injection of CO₂ together with an aqueous foaming agent
- Alternating the injection of CO₂ and an aqueous foaming agent

There are two types of foam; continuous-gas foam and discontinuous-gas foam (Falls et al. 1988). Continuous-gas foam (Figure 2.3) has gas channels in the foam that is not interrupted by lamellae. In discontinuous-gas foam (Figure 2.4) there are no gas channels. This type of foam can be divided into coarsely- and finely textured. In this type of foam the lamellae are stationary and they prevent the gas from flowing through the pore network.

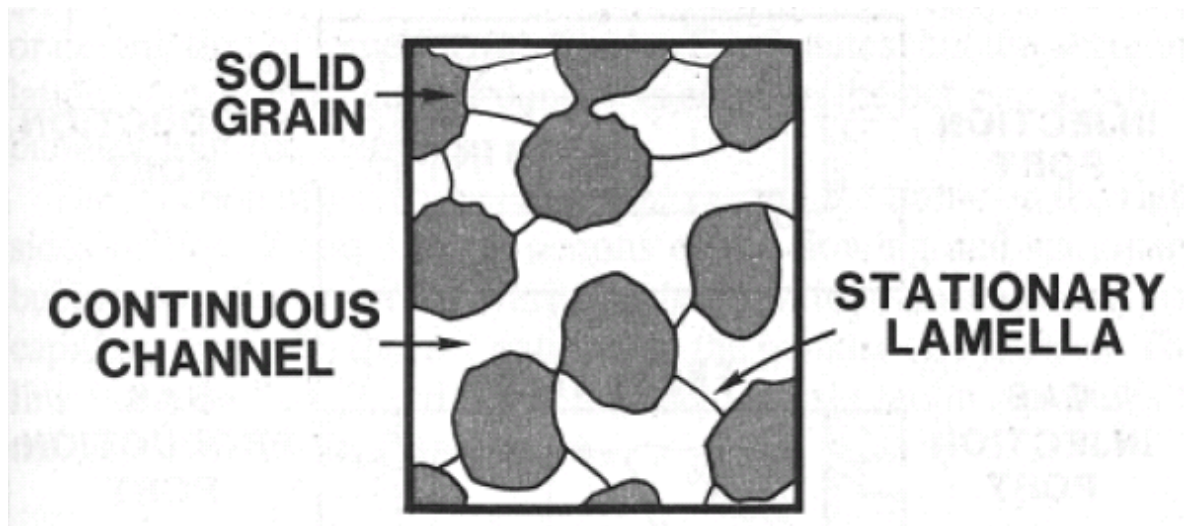


Figure 2.3: Continuous-gas foam in porous media (Falls et al. 1988).

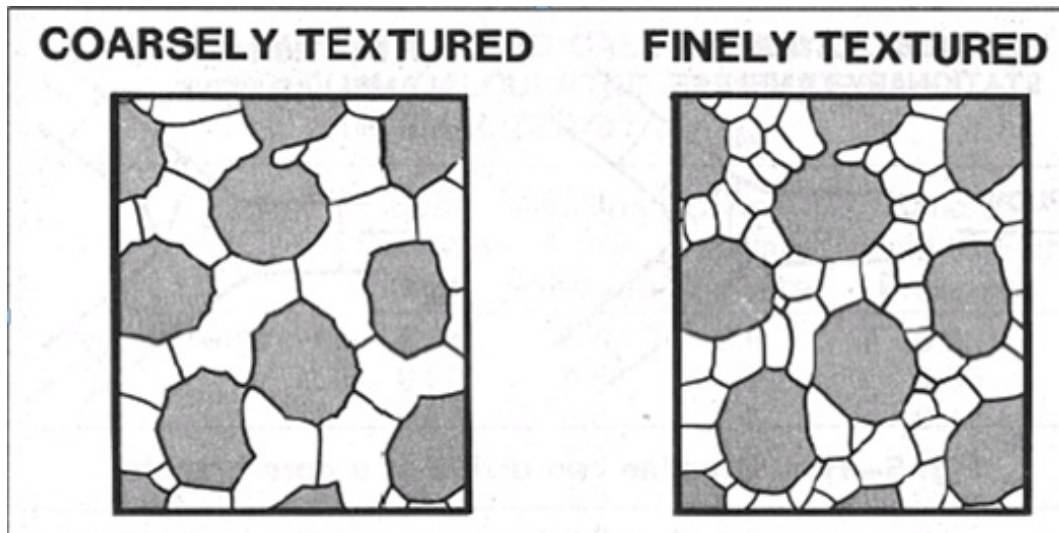


Figure 2.4: Discontinuous-gas foams, coarsely and finely textured (Falls et al. 1988).

In foam the apparent viscosity is increased and the relative permeability functions of the gas can be modified compared to if the gas was flowing alone (Panahi 2004). This can stabilize the displacement front and can lead to a reduced mobility and a higher oil recovery. Apparent viscosity of foam depends on the chemical structure and concentration of the foaming agent, foam quality i.e. gas fractional flow, flow rate, and the permeability of the reservoir rock (Lee et al. 1991). Hirasaki and Lawson presented in 1985 that foam texture, i.e. bubble size, was the most important variable affecting foam apparent viscosity in uniform, smooth capillaries. Foam with a finer texture has a larger resistance to flow. For a given foam texture the apparent viscosity is larger the higher the permeability (Lee et al. 1991, Yan et al. 2006). The dependence of permeability indicates that foam can divert flow from thicker to thinner fractures, and from high permeability matrix to low permeability matrix. The dynamic changes at gas/liquid interfaces of the bubble (Figure 2.5) are the factors that contribute to the apparent viscosity of foam (Hirasaki and Lawson 1985).

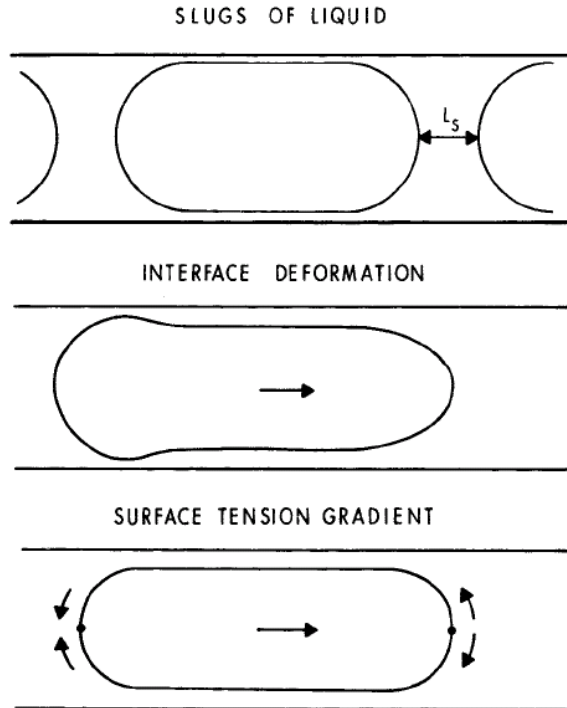


Figure 2.5: Mechanisms that affect apparent viscosity in smooth capillaries: slugs of liquid between the bubbles, resistance to deformation and the surface tension gradient (Hirasaki and Lawson 1985).

The resistance factor quantifies the effect of the foam if foam is generated (Chang and Grigg 1999). The presence of foam will create a pressure drop, and this is represented by the resistance factor (Chang and Grigg 1994). If the resistance factor is unity, there has not been generated foam. The resistance factor can show what effect the foaming agent have in controlling the CO₂ mobility (Kuehne et al. 1992, Chang and Grigg 1994).

In fractured reservoirs the aqueous foaming agent solution preferentially flows into the fractures, and this is where foam can form (Yan et al. 2006). This increases the local resistance to flow which decreases foam mobility. The local resistance is caused by viscous shear stresses in the lamellae between the pore walls and the gas/liquid interface, and the forces required to push lamellae through constricted pore throats (Nguyen et al. 2000). When the local resistance in the fractures is increased, CO₂-gas can be diverted by diffusion into matrix blocks that have a lower permeability; this increases the sweep efficiency (Casteel and Djabbarah 1988, Yan et al. 2006). The oil that has been retained in the matrix can be released by the injected CO₂-gas.

The efficiency of a CO₂-foam process in a fractured reservoir is dependent on the contact time and the transport of CO₂ from the fracture and into the oil in the matrix (Zuta et al. 2010a). There are physical and chemical mechanisms that influence the transport of CO₂-foam (Chung 1991). Some of the mechanisms are convective flow, dispersion, pore-throat filtration, pore-scale diffusion, retention and chemical reactions in the fractured media.

2.3 Foaming agent

The foaming agent can be a surfactant, macromolecules or finely divided solids (Schramm and Wassmuth 1994). In this thesis a surfactant will be used. Surfactants can reduce the surface tension and they can form a protective film at the bubble surfaces that can act as prevention to coalescence with other bubbles.

A surfactant can adsorb onto the surfaces or interfaces of a system and alter the interfacial properties when it exists at low concentrations in a system (Rosen 2004, Green and Willhite 1998). Surfactants consist commonly of a hydrocarbon portion and an ionic portion. The balance between the hydrocarbon portion and the ionic portion gives the surfactant its characteristics. Depending on the charge of the surfactant, it can be classified as anionic, cationic, nonionic or zwitterionic. The most frequently used ones in EOR processes are the anionic and nonionic surfactant (Green and Willhite 1998).

Surfactant is a very expensive chemical, but foam contains a relatively low concentration of surfactant in the aqueous phase and this can make the process cost-effective (Kovscek et al. 1993). The retention of surfactants in the reservoir, can lead to the stability of foam decreasing. Retention can make the process less cost-efficient, because the concentration of surfactant needs to be increased to make up for the loss. Loss of surfactant because of retention reduces the stability of the CO₂-foam, and cause the foam to collapse, and this can increase CO₂ mobility (Tabatabal et al. 1993).

Retention of surfactants depends on several parameters; surfactant concentration and structure, temperature, rock type, the presence of residual-oil phase, brine salinity and hardness, and wettability (Grigg and Mikhalin 2007). There are several different mechanisms where retention can happen depending on whether there is oil present or not in the reservoir (Mannhardt and Novosad 1994). If there is no oil present, the mechanisms can be;

- Adsorption onto solid/minerals
- Chemical degradation
- Precipitation during a chemical reaction in the reservoir

If oil is present, the foaming agent can also be retained by other mechanisms;

- Deactivation by binding to crude-oil asphaltenes
- Phase partitioning of the surfactant into the oil phase
- Adsorption onto the oil/water interface
- Coadsorption of the surfactant and oil components

In fractured reservoirs an additional retention mechanism can be a result of the surfactant being trapped inside the pores. The most critical type of retention for all types of reservoirs is adsorption. This is because it is the only mechanism that cannot be controlled by changing the type of surfactant. Adsorption of the surfactant happens because the surfactant interacts with the rock surface in such a way that the transport from the fracture network into the matrix block is delayed. The electrostatic attraction between the charged surface of the matrix and the charged head group of the surfactant molecule is one of the mechanisms that are responsible for the surfactant adsorption (Tabatabal et al. 1993).

The retention of the surfactant can be described with an adsorption isotherm (CMG Manual 2010.10). The adsorption isotherm is adsorption level as a function of fluid composition (Figure 2.6). The Langmuir isotherm correlation is a term that can describe the isotherms.

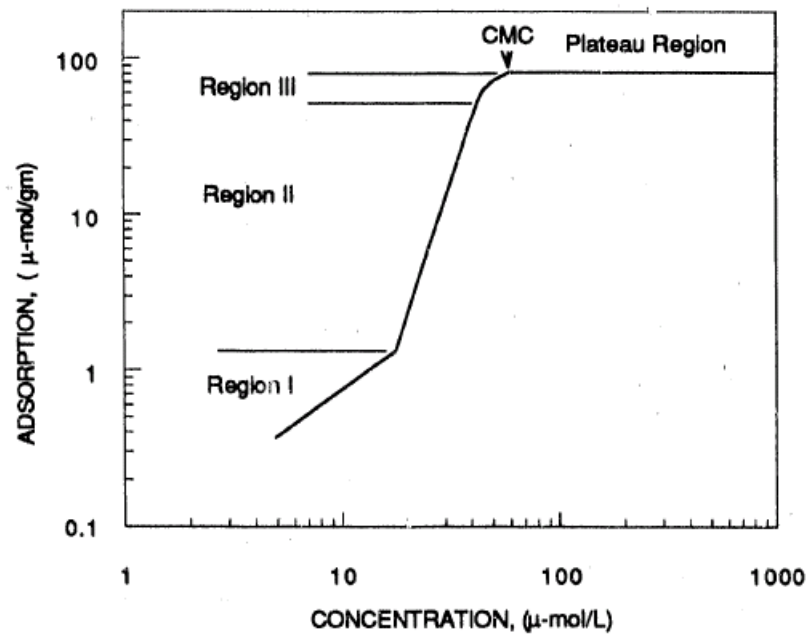


Figure 2.6: Typical adsorption isotherm for surfactant on mineral oxide surfaces (Scamehorn et al. 1982).

The adsorption isotherm can be divided into four regions (Figure 2.6) (Somasundaran and Fuerstenau 1966, Scamehorn et al. 1982). The first region, Region I, is at low surfactant concentrations. In this region the adsorption is described by Henry's Law. There are only unassociated, first layer surfactant molecules present on the surface. In Region II the adsorption increases faster. Lateral interaction between adsorbed surfactants, aggregates, results in hemimicelles that first appear on the most energetic surface patches. Region III is at higher surfactant concentrations, and here the adsorption increases slowly. Forming of hemimicelles happens on less energetic patches. Eventually the critical micelle concentration (CMC) of the surfactant is reached, and above this concentration, the adsorption is independent of concentration. This is the Plateau Region.

In the following chapters the procedures, results, discussion and conclusions from this study on retention in a fractured chalk model will be presented.

3. Experiments

3.1 Porous media

The core plugs were prepared from Liège outcrop chalk which was used as analogous to the reservoir chalks in the North Sea. Common Liège chalk properties are that the porosity is approximately 40 % and the permeability is approximately 1 – 2 mD (Strand et al. 2007). Liège chalk contains small amounts of clay and less than 2 wt% silica. The chalk is from Lixhe in Belgium, and the age is Upper Campanian. Core plugs that were used in the experiments had dimensions similar; the length was approximately 7.0 cm and the diameter was approximately 3.8 cm.

3.2 Chemicals and fluids

An anionic surfactant was the foaming agent used in the experiments. The surfactant was an internal olefin sulfonate (IOS) with $C_{11} - C_{12}$ carbon chain length. It will be referred to as S5, according to internal IRIS rules. The surfactant was obtained from the supplier with an activity of 24.8 wt%. The foaming agent solution used in laboratory experiments was prepared by dissolving a specific volume of the surfactant in sea water. The active concentration of S5 in the prepared foaming agent solution was determined to be approximately 0.86 wt%.

Synthetic formation water (FW), sea water (SW) and sea water with lithium (SWL) was prepared (Table 3.1). Core plugs were prepared by using FW and the SW was the brine used

to prepare the foaming agent solution in the fractured chalk model experiments. During the flow-through retention experiments SWL was used to prepare the foaming agent solution. Lithium was the tracer because it does not react with the chalk or the surfactant. All brines were filtered with a 0.45 µm HAWP filter before they were used.

The stock tank oil that was used in the core plug preparations was from a North Sea field.

Table 3.1: The compositions of the brines used in the experiments.

Salt	Formation water (FW) [g/l]	Sea water (SW) [g/l]	SW with SO ₄ ²⁻ and Li (SWL) [g/l]
NaCl	40.00	23.38	23.38
Na ₂ SO ₄	-	3.41	3.41
NaHCO ₃	-	0.17	0.17
KCl	0.31	0.75	0.75
MgCl ₂ *6H ₂ O	5.00	9.05	9.05
CaCl ₂ *2H ₂ O	34.00	1.91	1.91
LiCl	-	-	0.09

3.3 Preparation of core plugs with FW

The procedure for preparing and saturating the core plugs with FW was:

1. The dimensions and weights of the core plugs were determined.
2. The core plugs were then heated to 120 °C until the weight was constant.
3. A desiccator (Figure 3.1) was used to saturate the core plugs with FW. Vacuum removed all the air inside the core plugs, and then the core plugs were saturated with FW by introducing the FW to the desiccator. The core plugs were left over night in the desiccator.

- The weight of the 100 % water saturated core plugs was determined. The pore volume and porosity were then calculated based on the density of FW.



Figure 3.1: The desiccator that was used to saturate the core plugs.

Sulfate can sometimes be found in Liège plugs and this has been found to change the wettability to water-wet during aging with crude oil (Fjelde 2008). The core plugs were therefore flooded with approximately 8 – 10 pore volumes of FW until there was no detection of sulfate in effluent samples. Figure 3.2 shows the set-up.

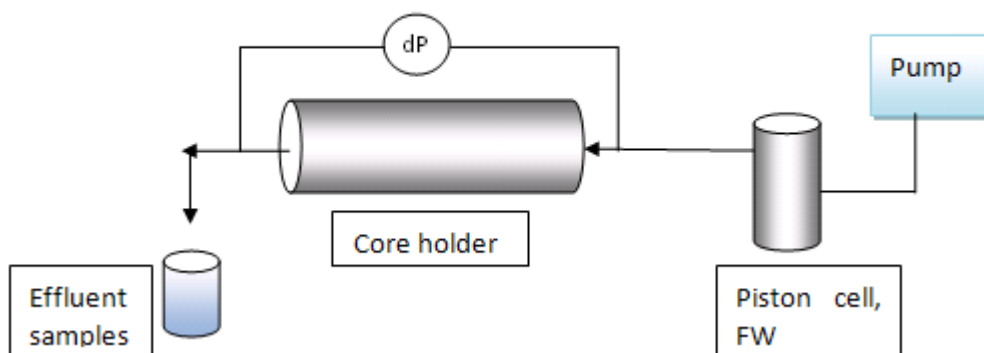


Figure 3.2: Core flooding rig used during core cleaning and permeability determination.

The absolute permeability (k_{abs}) of the core plugs was determined by injecting FW with rates of 5 - 10 ml/min until a stable differential pressure was reached (Figure 3.2). This was done with an overburden pressure of 10 bar and at room temperature.

3.4 Preparation of core plugs with stock tank oil

The core plugs at S_{wi} were prepared in another project at IRIS. The core plugs were drained with nitrogen to S_{wi} by using the unconfined porous disc method and the wettability of the core plugs were established by aging with stock tank oil at 90 °C. This method has earlier been described (Fjelde et al. 2008a, 2008b).

The core plugs were water flooded with SW at injection rates of 0.1, 0.2 and 0.5 ml/min until there was no more oil produced. During the water flooding the differential pressures was monitored. From this the water and oil productions and end point permeability ($k_{rw}(S_{orw})$) at S_{orw} were determined.

3.5 Static retention experiments; fractured chalk model

3.5.1 Preparation of fractured chalk model

The experiments were carried out in fractured chalk models (Figure 3.3). Core plugs were placed into plastic containers with an inside diameter of 5.2 cm. This creates a 1.4 cm, or 0.7 cm x 2, annulus space around the core plug, between the core plug and the wall of the container. This annulus space was an artificial fracture. In the bottom of the container there were glass beads placed, this was because transportation into the core plug should be able

to occur on all the surface area, including the bottom. The foaming agent solution was filled in the fracture and the concentrations of the foaming agent in the fracture were monitored over time. The initial concentration of the foaming agent was set to 0.86 wt%. The core plugs that were used were at 100 % water saturation or at S_{orw} . Figure 3.4 shows the different designs of the core plugs that were used in the experiments.

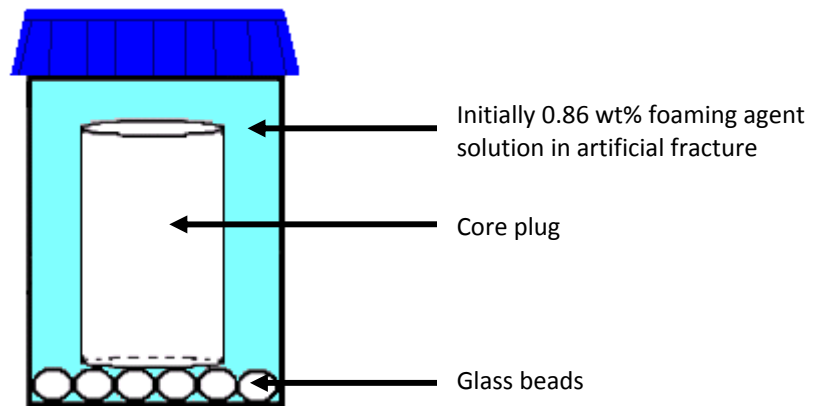


Figure 3.3: Sketch of the fractured model used in experiments and simulations. The light blue area was where the foaming agent solution was filled initially.

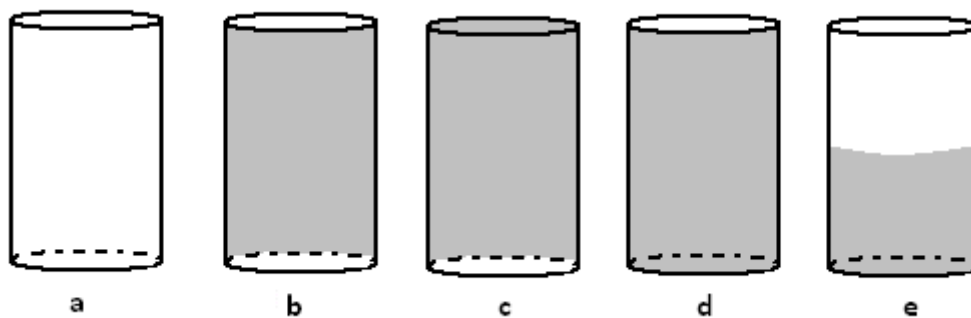


Figure 3.4: Sketches of the different designs used in the fractured model experiments and simulations. The grey shading shows the blocked surface areas; a) No surface area is blocked, b) The lateral surface area, c) The top and lateral surface area, d) The bottom and the lateral surface area, e) The bottom and half of the lateral surface area.

The fractured model was placed in a heating cabinet at 55 °C and 1 atm. The pressure was assumed to not be important for the retention process as long as pH did not affect the retention.

Teflon-tape and shrinking-teflon were used to block the different surface areas of the core plugs (Figure 3.5). The shrinking-teflon was heated such that it shrunk in size, and surrounded/covered the core plug. The experiments were performed with parallel core plugs.

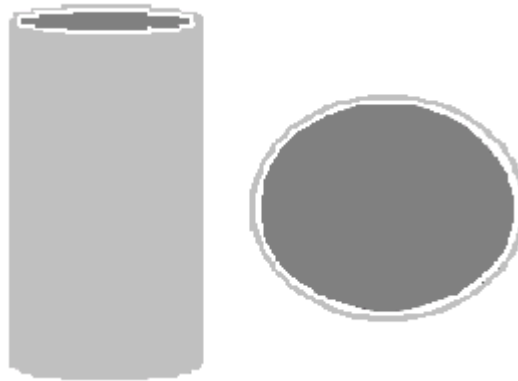


Figure 3.5: Sketch of the core plug that had the lateral surface area blocked, seen from the side and from the top. The dark-grey area is the core plug, the white area is the teflon-tape and the light-grey is the shrinking-teflon.

3.5.2 Procedure for static experiments

The procedure for the static retention experiments was:

1. The artificial fracture around the core plug was filled with 0.86 wt % foaming agent solution.
2. The core plugs was placed in an oven at 55 °C.
3. Liquid samples of approximately 1.5 ml were taken out from the space above the core plug at regular intervals and analyzed for foaming agent concentration.
4. This was done for approximately 60 days.

3.6 Static adsorption experiment

The static adsorption experiment was done to find the adsorption isotherm. This was determined because it was an important input in STARS (section 4.1).

The procedure was (Zuta and Fjelde 2009, Zuta et al. 2010b):

1. Approximately 5 g of Liège chalk was crushed and mixed together with approximately 15 g of foaming agent solution.
2. Foaming agent solutions with different concentrations were used; 1 wt%, 0.7 wt%, 0.5 wt%, 0.3 wt%, 0.2 wt% and 0.1 wt%.
3. This was mixed together over night at two different temperatures; room temperature and 55 °C.
4. The concentration of foaming agent was determined with two-phase titration.
5. The adsorption isotherm was then determined.

3.7 Flow-through retention experiments

The flow-through retention experiments were done on core plugs at 100 % water saturation or at S_{orw} . The active foaming agent solution with a concentration of 0.86 wt% was injected into the core plugs together with a tracer, lithium, at an injection rate of 0.2 ml/min. A flooding rig similar to the one in Figure 3.2 was used in the experiment. The main difference from the flooding rig in Figure 3.2 was that in this experiment the core holder was placed inside an oven. The experiment was done until the effluents and the injected foaming agent concentrations were equal. An auto sampler collected the effluents, and the samples were analyzed for concentration of foaming agent and lithium.

3.8 Analytical methods

3.8.1 Two-phase titration with Hyamine

Two-phase titration was used to determine the concentration of the foaming agent during the experiments. A cationic dye, Methylene blue (MB), was used as indicator. The organic phase was chloroform, and the titrant was Hyamine. Hyamine is a cationic surfactant which consists of a single pure compound.

The titration is based on the reaction where an anionic surfactant forms an ion pair with a cationic surfactant (Schmitt 1992). In the beginning the MB is in the organic phase with the anionic surfactant. As more Hyamine is added, the MB ion gets displaced from the complex by Hyamine, and MB is extracted from the organic phase into the aqueous phase. When the blue colors of the aqueous and organic phase have the same intensity, the end point is reached.

The procedure was:

1. A sample of 0.1 g foaming agent solution together with 1.50 ml chloroform and 4.0 ml MB solution were added to a test tube with screw stopper.
2. A $4 \cdot 10^{-3}$ M solution of Hyamine was added until the colors of the phases were equal.

3.8.2 Sulfate analysis

A Sulfate Cell Test Kit was used to determine the sulfate concentration (Merck 2003). The samples were added in the Sulfate Cell Test Kit together with Bariumchloride-2-hydrate. If there was sulfate ions present in the sample, they would precipitate with barium ions according to the reaction:



The Spectroquant NOVA60 photometer measured the resulting turbidity at wavelength 470 nm. Merck has given the following information about the method: the measuring range is 5-250 ppm, standard deviation is ± 2.8 ppm and the confidence interval is ± 7 ppm.

The procedure was:

1. Approximately 1 ml of the sample was added to the test kit.
2. 4 ml of FW was added to dilute the sample.
3. A spoonful of Bariumchloride-2-hydrate was added to the test kit and immediately stirred for exactly 20 seconds.
4. The sample was then left to rest for exactly 2 minutes. A timer was used to ensure that each sample got the exact same treatment.
5. The sulfate concentration was immediately measured by the spectrophotometer.

3.8.3 Lithium analysis

An external laboratory determined the lithium concentration using Inductive Coupled Plasma (ICP) method. The results had an insecurity of $\pm 15\%$.

4. Numerical simulation

4.1 Introduction

The simulations were done with the reservoir simulator STARS, a modeling tool from CMG. STARS is a thermal and stream additive simulator that can simulate with three-phase multi-components (CMG Manual 2010.10). The transport of the foaming agent was assumed to occur by adsorption and diffusion from the fracture into the matrix rock.

It is required that there is a description of the adsorption of the foaming agent component in the model. To do this, the model needs a set of constant temperature adsorption isotherms as input (CMG Manual 2010.10).

Molecular diffusion in STARS can be modeled with any component and any phases (CMG Manual 2010.10). The simulation can be done with different values for each grid block for each grid direction. The diffusion is temperature and viscosity dependent.

4.2 Simulation setup

A radial model was used that had grid blocks that were 50*1*100, which represented the container in which the core plugs were (Figure 3.3). The core plug was a 41*1*88 part of the model, and the rest was the artificial fracture (Figure 4.1). The core plug part of the model was given the average porosity and permeability values measured from the experiments. The core plugs were either at 100 % water saturation or at S_{orw} . The artificial fracture was

given a porosity of 0.99 and a permeability of 1000 mD, and it was initially filled with a foaming agent solution with a concentration of 0.86 wt%.

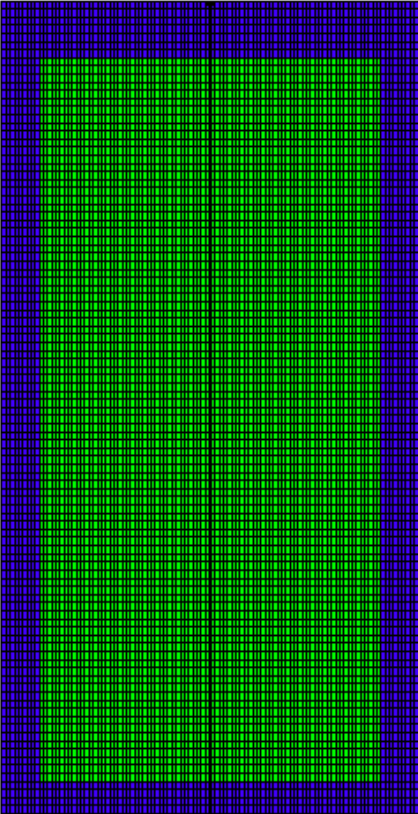


Figure 4.1: The grid established in STARS. The blue area is the artificial fracture and the green area is the core plug.

During the simulations in STARS the different designs (Figure 3.4) were created by setting the transmissibility to zero on the surface area that was to be blocked. The concentration of the foaming agent in the fracture was monitored over time for the different designs. It was decided to take samples over the core plug. In the design where the lateral surface area was blocked (Figure 3.4b), the foaming agent concentration right under the core plug, on the side of the core plug and some concentrations inside the core plug was plotted in addition (Figure 4.2).

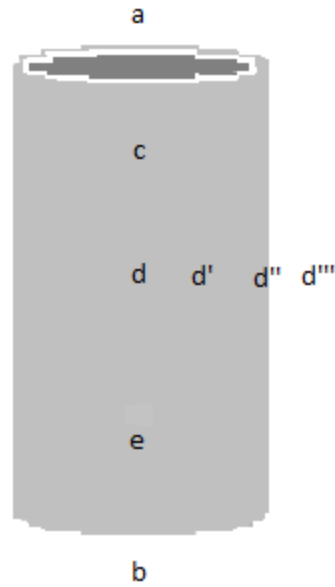


Figure 4.2: Location of the concentration points of interest in the design were the lateral surface area was blocked.

The adsorption isotherm that was needed in STARS was found experimentally (section 3.6). This experiment was done to be able to start the simulations with STARS before the fractured model had reached the foaming agent equilibrium concentration.

There was performed some simulations on the core plug with lateral surface area and bottom blocked (Figure 3.4d) at 100 % water saturation with different core plug lengths on a larger scale. The diameter of the core plug was constant at 30 cm, and the length varied; 30 cm, 50 cm and 70 cm.

5. Results

The properties of the core plugs that were used in the fractured model experiments were as presented in Table 5.1 and Table 5.2. All the core plugs had a diameter of approximately 3.8 cm and a length of approximately 7.0 cm. The porosity of the core plugs ranged between 40 – 43 %. k_{abs} was only measured for two of the core plugs at 100 % water saturation and was approximately 0.7 mD. The core plugs at S_{orw} had k_{abs} that were approximately 1.8 mD.

Table 5.1: The properties of the core plugs at $S_w = 100\%$ used in fractured models.

Name	Length [cm]	Diameter [cm]	Porosity [%]	k_{abs} [mD]	Comment (see Figure 3.4)
AH16	7.01	3.81	40.20	0.63	No blockage
A22	7.02	3.81	40.00	0.71	No blockage
AH25	7.05	3.80	39.90	-	Lateral surface blocked
A26	7.04	3.80	39.84	-	Lateral surface blocked
A27	7.00	3.80	40.06	-	Bottom and half lateral surface blocked
A28	7.02	3.82	40.00	-	Bottom and half lateral surface blocked
A29	7.04	3.80	41.73	-	Lateral surface and top blocked
A31	7.08	3.80	41.60	-	Lateral surface and top blocked
A32	7.06	3.81	41.10	-	Lateral surface and bottom blocked
A33	7.08	3.81	42.18	-	Lateral surface and bottom blocked

Table 5.2: The properties of the core plugs at S_{orw} used in fractured models.

Name	Length [cm]	Diameter [cm]	Porosity [%]	k_{abs} [mD]	Comment (see Figure 3.4)	S_{wi} [%]	S_{orw}	$k_{ro}(S_{wi})$	$k_{rw}(S_{orw})$
FB29	7.11	3.82	43.12	1.83	Lateral surface and bottom blocked	15.58	30.35	0.37	0.43
FB30	7.09	3.81	42.12	1.87	Lateral surface blocked	17.25	23.94	0.32	0.32

The flow-through retention experiments were done to determine the retention of foaming agent in dynamical experiments. Table 5.3 and 5.4 show the properties of the core plugs that were used in the flow-through retention experiments.

Table 5.3: The properties of core plugs at $S_w = 100\%$, flow-through experiment.

Name	Length [cm]	Diameter [cm]	Porosity [%]	k_{abs} [mD]
J1	7.12	3.80	40.27	0.91
J3	7.10	3.80	40.11	1.11

Table 5.4: The properties of the core plugs at S_{orw} , flow-through experiments.

Name	Length [cm]	Diameter [cm]	Porosity [%]	k_{abs} [mD]	S_{wi} [%]	S_{orw}	$k_{ro}(S_{wi})$	$k_{rw}(S_{orw})$
D1	7.08	3.81	44.00	1.83	15.06	19.87	1.79	0.43
D2	7.06	3.81	44.00	1.87	14.02	16.10	1.74	0.54

5.1 Experimental results from fractured model experiments

The fractured model experiments were first done with epoxy-glue as blocking agent on the core plug. The results were then not reasonable. The method was therefore tested by blocking all the sides of the core plug with the glue, and the concentration should then be constant over night. This was not the case. The reason for this could either be that the foaming agent was adsorbed onto the surface area of the glue, or the glue did not block the surface area good enough so the foaming agent could still be transported into the core plug. The solution to this was to start over again, with another way of blocking the surface areas; shrinking-teflon and teflon-tape (Figure 3.5).

Experiments on the fractured model were done over a period of approximately 60 days. Samples were taken out periodically over the core plug, and analyzed for foaming agent

concentration. The concentration of the foaming agent was plotted vs. time. The transport of the foaming agent was expected to occur because of retention and molecular diffusion of the foaming agent from the fracture into the matrix. The concentration of the foaming agent in the fracture and the transport time was expected to be dependent on the different designs.

5.1.1 No surface area blocked

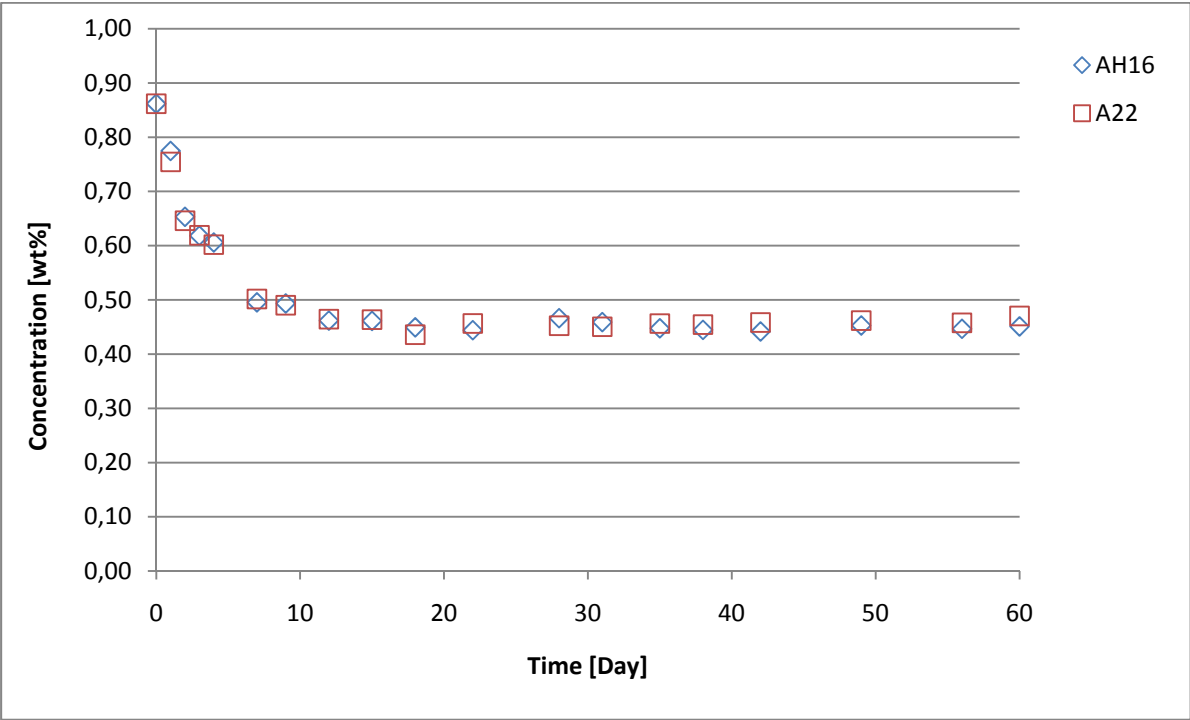


Figure 5.1: Foaming agent concentration vs. time for the two parallel core plugs with no surface area blocked, $S_w = 100\%$.

The base case fractured model at 100 % water saturation is shown in Figure 5.1. In this design, all the surface areas were open and exposed to the foaming agent solution (Figure 3.4a). The foaming agent was expected to be transported from the fracture into the core plugs from all sides. As shown in Figure 5.1, the foaming agent concentration decreases fast the first 8 – 10 days, and then the concentration starts to stabilize at a concentration of

approximately 0.45 wt% in the fracture. The concentration was constant throughout the rest of the experimental time, and equilibrium was assumed to be achieved. The two parallel core plugs had similar foaming agent concentrations throughout the experiments.

5.1.2 Lateral surface area blocked

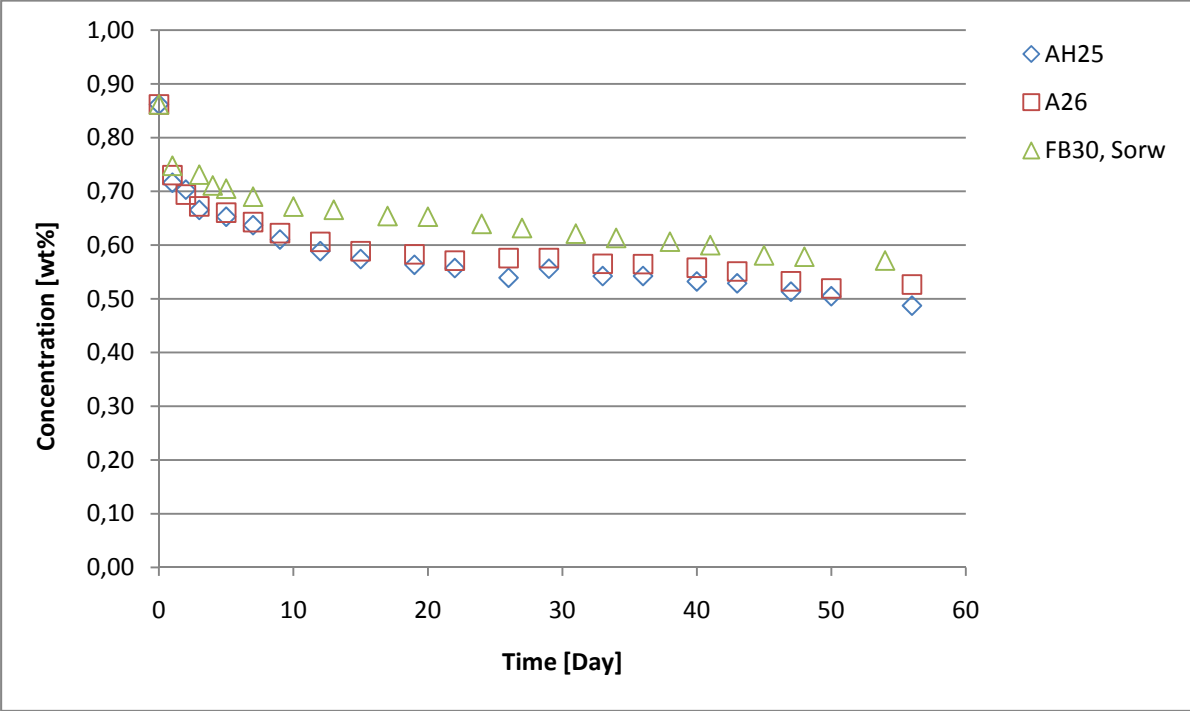


Figure 5.2: Foaming agent concentration vs. time for the two parallel core plugs, AH25 and A26, with the lateral surface area blocked at $S_w = 100\%$. The figure also show the foaming agent concentration vs. time for the core plug at S_{orw} , FB 30, with the lateral surface area blocked.

The experiments with lateral surface area blocked are shown in Figure 5.2. Here the foaming agent was expected to be transported into the core plug through the top surface area and the bottom surface area (Figure 3.4b). Included is also a similar experiment with a core plug at S_{orw} . The concentration of foaming agent in both cases decreased fast the first 10 – 12 days, and then the reduction was much slower. The parallel core plugs with 100 % water saturation (AH25 and A26) had similar foaming agent concentration throughout the

experiments. The concentration at the end of the experiments was approximately 0.51 wt% for AH25 and A26. Compared with the base case at 100 % water saturation it is seen that equilibrium is not reached for this design. The concentrations are expected to continue to decrease until it has reached an equilibrium concentration of approximately 0.45 wt%. The core plug at S_{orw} (FB30) followed the same trend as the core plugs at 100 % water saturation. The difference was that the concentrations for the core plug at S_{orw} were slightly higher than the core plugs at 100 % water saturation. This might be due to less accessible pore volume in the core plug at S_{orw} , and/or the oil occupies some of the surface area in the chalk where the foaming agent could have been retained. The concentration at the end of the experiments for the core plug at S_{orw} was 0.57 wt%.

5.1.3 Lateral surface area and top blocked

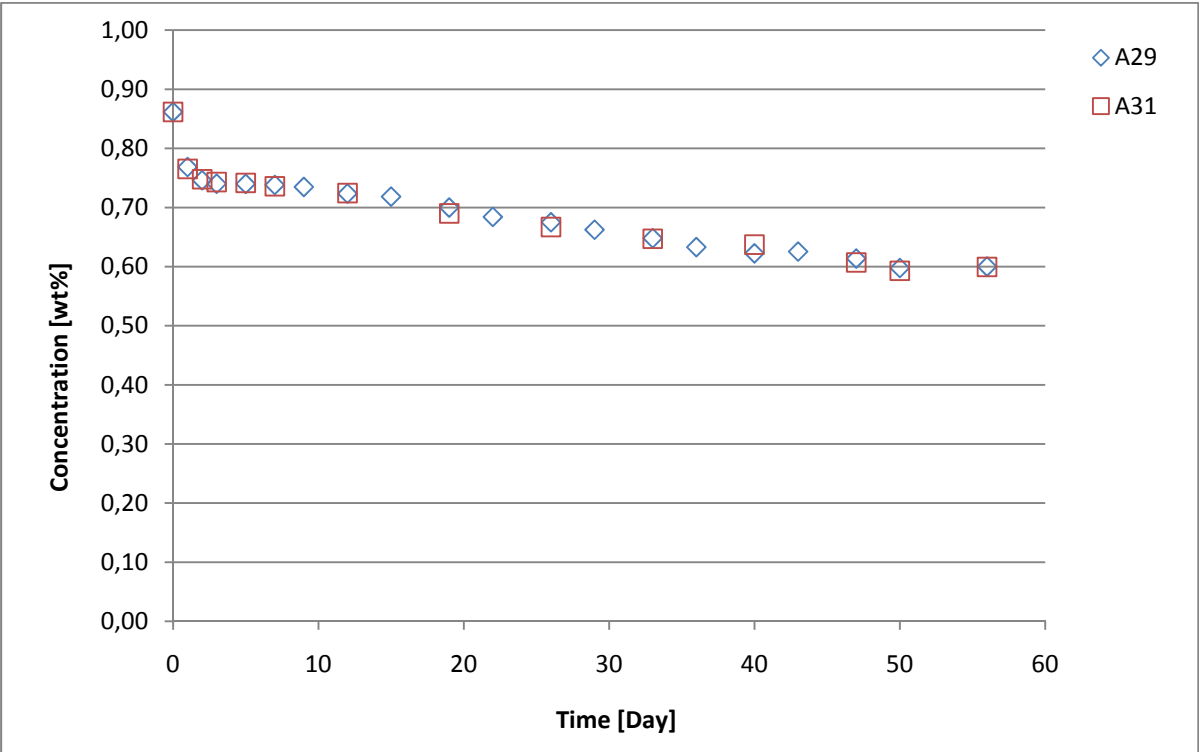


Figure 5.3: Foaming agent concentration vs. time from the two parallel core plugs, A29 and A31, with the lateral surface area and the top blocked at $S_w = 100\%$.

Figure 5.3 shows the design when the foaming agent only can be transported through one surface area; the bottom. Figure 3.4c shows a sketch of the design. There was not sampled each time for A31 because there was not that much foaming agent solution above the core plug in the container. The concentrations of foaming agent for the two parallel core plugs, A29 and A31, were similar during the experiments. In this case the concentration decreased fast the first day, and then it decreases more slowly during the rest of the experiments. The concentration at the end of the experiments was 0.60 wt%. Equilibrium concentration has not been reached compared to base case, and the concentration is expected continue to decrease until it reaches the equilibrium concentration seen in the base case.

5.1.4 Lateral surface area and bottom blocked

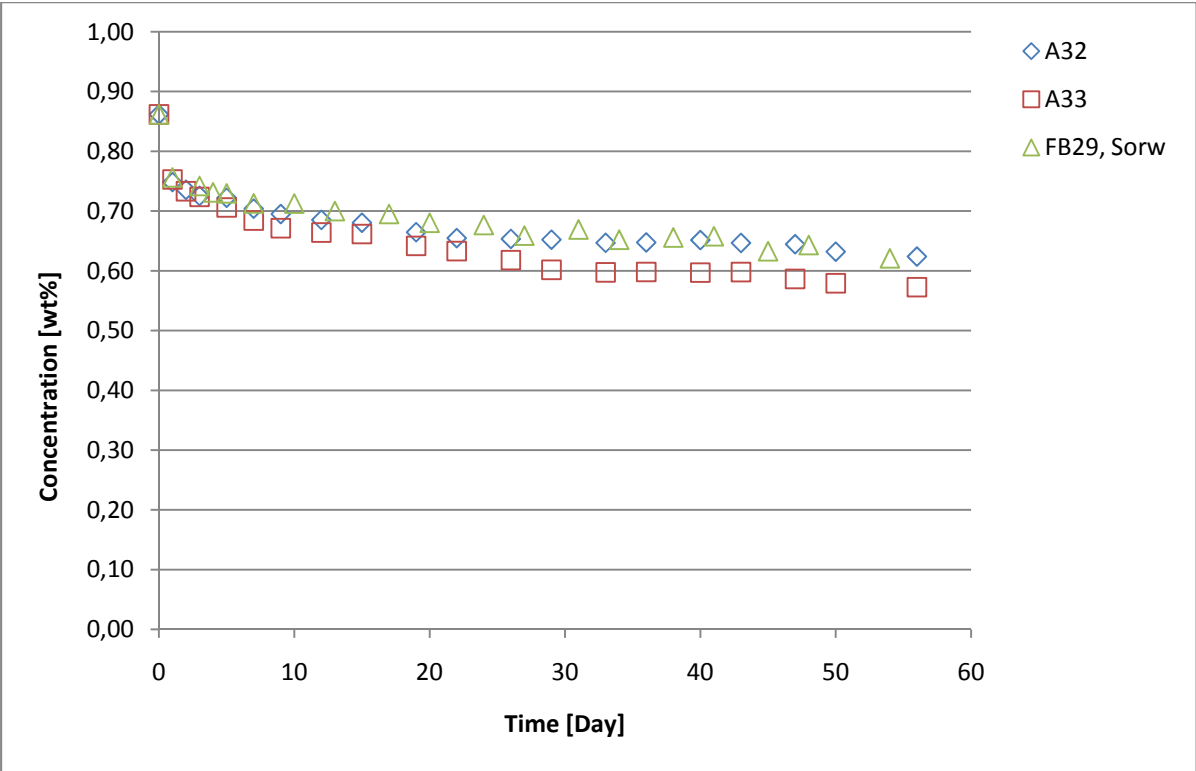


Figure 5.4: Foaming agent concentration vs. time for the two parallel core plugs, A32 and A33, at $S_w = 100\%$ with the lateral surface area and the bottom blocked. The figure also show foaming agent concentration vs. time for the core plug at S_{orw} , FB29, with the lateral surface area and bottom blocked.

In Figure 5.4 the top surface area is exposed to the foaming agent solution (Figure 3.4d). It was seen that there was not much difference between the core plugs that had 100 % water saturation, A32 and A33, and the core plug at S_{orw} , FB29. The concentration of foaming agent decreased fast the first day, and then it decreased more slowly until 30 days, after this the concentration decreased very slowly. As seen in Figure 5.4, the two parallel cores (A32 and A33) at 100 % water saturation started to differ slightly around 30 days. This could be because of measuring error in the titration, permeability difference between the core plugs, or the shrinking-teflon may not have been completely tight in core plug A33. Average concentration at the end of the experiment for the core plugs at 100 % water saturation was 0.60 wt%. The equilibrium concentration has not been reached for this design compared to the base case at 100 % water saturation in Figure 5.1. The concentration profile for the core plugs at 100 % water saturation and the core plug at S_{orw} had the same trend, and there was only a small difference in concentration between them. The concentration at the end of the experiments for the core plug at S_{orw} was 0.62 wt%.

5.1.5 Half the lateral surface area and bottom blocked

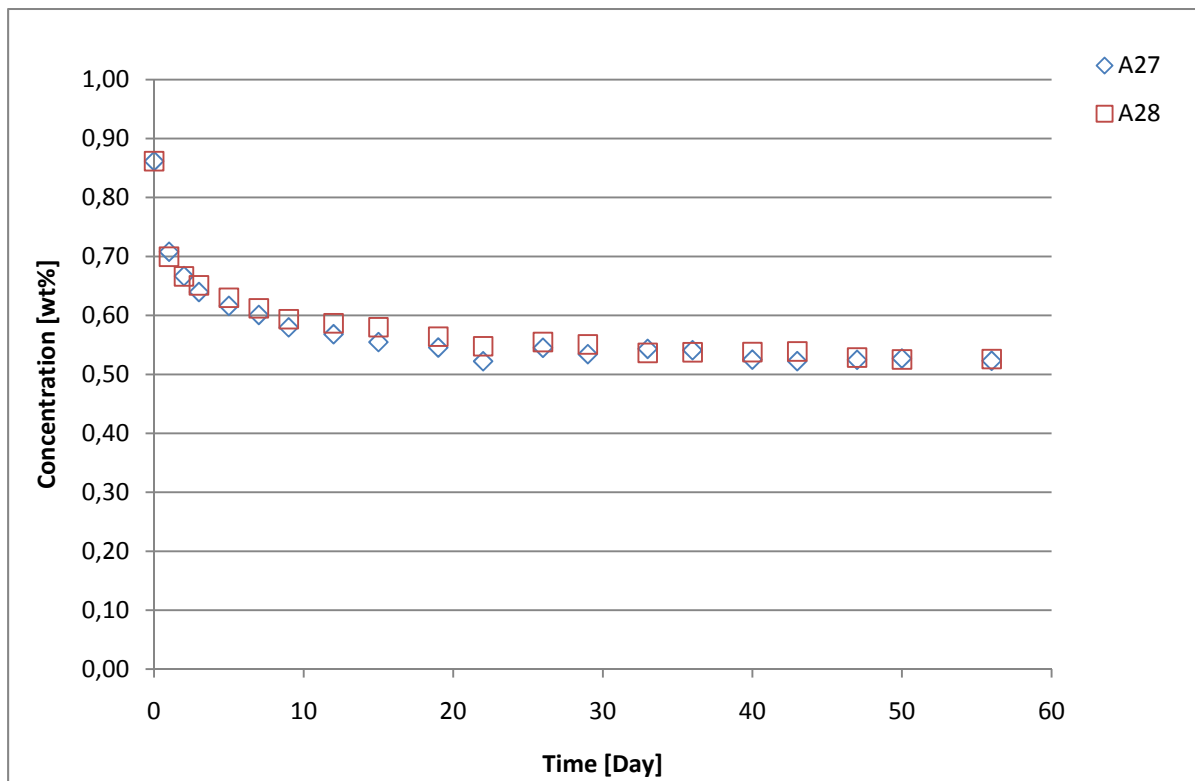


Figure 5.5: Foaming agent concentration vs. time for the two parallel core plugs, A27 and A28, at $S_w = 100\%$, and half the lateral surface area and the bottom is blocked.

The core plugs where the foaming agent could be transported through half of the top lateral surface area and the top surface area are shown in Figure 5.5. The sketch of this design is seen in Figure 3.4e. The concentrations of foaming agent in the two parallel core plugs, A27 and A28, were similar. The concentration decreased fast the first 15 - 20 days, and then the concentration decreased more slowly. The concentration at the end of the experiments was 0.52 wt%. Compared to the base case (Figure 5.1), the equilibrium concentration had not been reached at approximately 55 days. The concentration of foaming agent in the fracture is expected to continue to decrease until it reaches approximately 0.45 wt%.

5.1.6 Summary of the experimental results

Retention includes all the mechanisms that hold the foaming agent trapped inside the pores. In the fractured model it is the total amount of foaming agent present inside the core plug. The retention of foaming agent (R) in the different cases can be found with the equation:

$$R = \frac{([FA]_{Initial} - [FA]_{End}) \cdot W_{FAS}}{W_{rock}} \quad (6)$$

Here $[FA]_{Initial}$ and $[FA]_{End}$ is the foaming agent concentration initially and at the end respectively, and W_{FAS} and W_{rock} is the weight of foaming agent solution in the artificial fracture and core plug respectively. Initial foaming agent concentration is 0.86 wt%. W_{FAS} is the volume of foaming agent solution multiplied by the density of this solution.

If equilibrium is reached, the adsorption of foaming agent can be found. Adsorption is the amount of foaming agent that is adsorbed onto solids or minerals, i.e. the amount of foaming agent in the pores is not included. At equilibrium it is assumed that all the FW inside the core plug has been mixed with the foaming agent solution. The foaming agent concentration due to dilution, $[FA]_{diluted}$, can be calculated with the equation:

$$[FA]_{diluted} = [FA]_{Initial} \cdot \frac{V_{fracture}}{V_{fracture} + V_{PV}} \quad (7)$$

Here $V_{fracture}$ is the volume of the artificial fracture and V_{PV} is the pore volume of the core plug. The weight of the foaming agent solution at equilibrium, W_{FAS}^{eq} , is:

$$W_{FAS}^{eq} = W_{FAS} + W_{PV} \quad (8)$$

The W_{PV} is the weight of the FW in the pore volume of the core plug. The equation used to find the adsorption of foaming agent at equilibrium, A , is:

$$A = \frac{([FA]_{diluted} - [FA]_{End}) \cdot W_{FAS}^{eq}}{W_{rock}} . \quad (9)$$

The different foaming agent concentrations at the end of the experiments and the retention of the foaming agent are presented in Table 5.5 and 5.6. In Table 5.5 the designs at 100 % water saturation are compared, and in Table 5.6 the core plugs at S_{orw} are compared with the core plugs at 100 % water saturation that have the same design.

Table 5.5: Summary of the designs with $S_w = 100\%$.

Designs (Figure 3.4), $S_w = 100\%$	End concentration, [wt%]	Retention of foaming agent, [mg/g rock]	Adsorption of foaming agent, [mg/g rock]
No blockage	0.45	3.47	2.31
Lateral surface area blocked	0.51	2.96*	-
Half the lateral surface area and bottom blocked	0.52	2.88*	-
Lateral surface area and top blocked	0.60	2.20*	-
Lateral surface area and bottom blocked	0.60	2.20*	-

* Equilibrium is not reached.

Table 5.6: Comparison of cases with $S_w = 100\%$ and S_{orw} .

Case	Saturation	End concentration, [wt%]	Retention of foaming agent, [mg/g rock]
Lateral surface area blocked	$S_w = 100\%$	0.51	2.96*
	S_{orw}	0.57	2.51*
Lateral surface area and bottom blocked	$S_w = 100\%$	0.60	2.20*
	S_{orw}	0.62	2.08*

* Equilibrium is not reached.

Table 5.5 shows that there is a connection between how much surface area that is exposed to the foaming agent solution and the change in concentration of the foaming agent in the fracture over time. The time until the concentration is at equilibrium is dependent on what

type of surface area that is exposed. This is because the foaming agent solution has different transportation lengths in the different designs, and that affects the time until the core plug is completely saturated. In Table 5.6 it is shown that there is a very small difference in end concentration and retention of foaming agent for the different designs at 100 % water saturation and at S_{orw} for the foaming agent used in these experiments. For other types of foaming agents there has been reported that there is an effect of oil on the retention (Zuta et al. 2010b). The concentration at the end of the experiments for FB29 and FB30 cannot be compared to an equilibrium concentration because it is difficult to predict if the experimental results at S_{orw} will continue to follow the results from the core plugs at 100 % water saturation.

It is assumed that the design where no surface area is blocked had reached equilibrium after 60 days, and maximum retention of the foaming agent is therefore 3.47 mg/g rock. This gives an adsorption of foaming agent of 2.31 g/g rock. The adsorption in the other designs is expected to reach this value after a longer period of time.

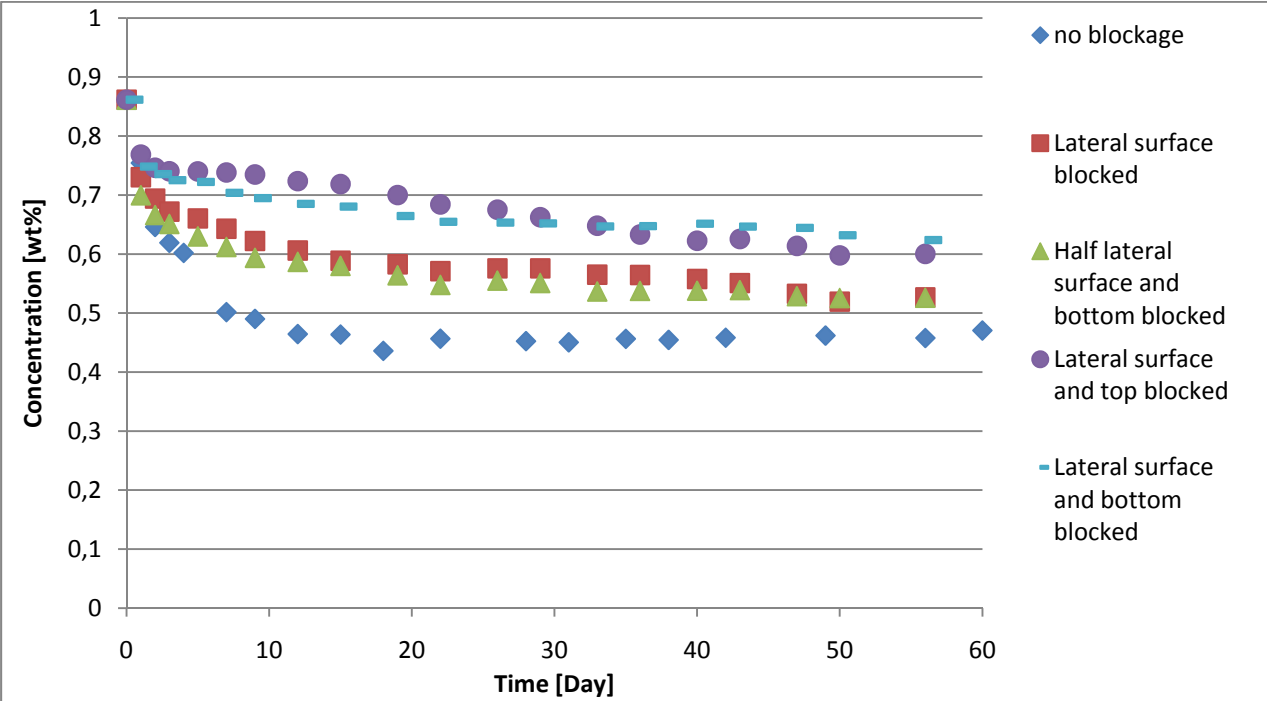


Figure 5.6: Foaming agent concentration vs. time for all of the designs plotted together at $S_w = 100\%$.

Figure 5.6 show a plot of the concentration changes in the fractures vs. time for one core plug in each design at 100 % water saturation. It is seen that the larger the surface area exposed to the foaming agent solution was, the faster the foaming agent concentration decreased, and the faster the foaming agent was adsorbed in the core plug. The type of surface area blocked had an impact on the time it took until the equilibrium concentration for the foaming agent was reached because of the different transportation lengths.

5.2 Static adsorption experiment

The adsorption isotherm for the foaming agent was found in the static adsorption experiment at 100 % water saturation. Figure 5.7 shows the adsorption isotherm in simulation units, and Figure 5.8 shows the adsorption isotherm in experimental units. The Figures show that the adsorption of the foaming agent onto crushed chalk rock decreases with increasing temperature. This happens because adsorption is an exothermic process (Mannhardt and Novosad 1994). The adsorption of the foaming agent reaches equilibrium adsorption between 0.4 – 1.0 wt% at 55 °C. At room temperature, the adsorption seems to increase with increasing concentration of the foaming agent. The adsorption isotherm at 55 °C was used in the simulations.

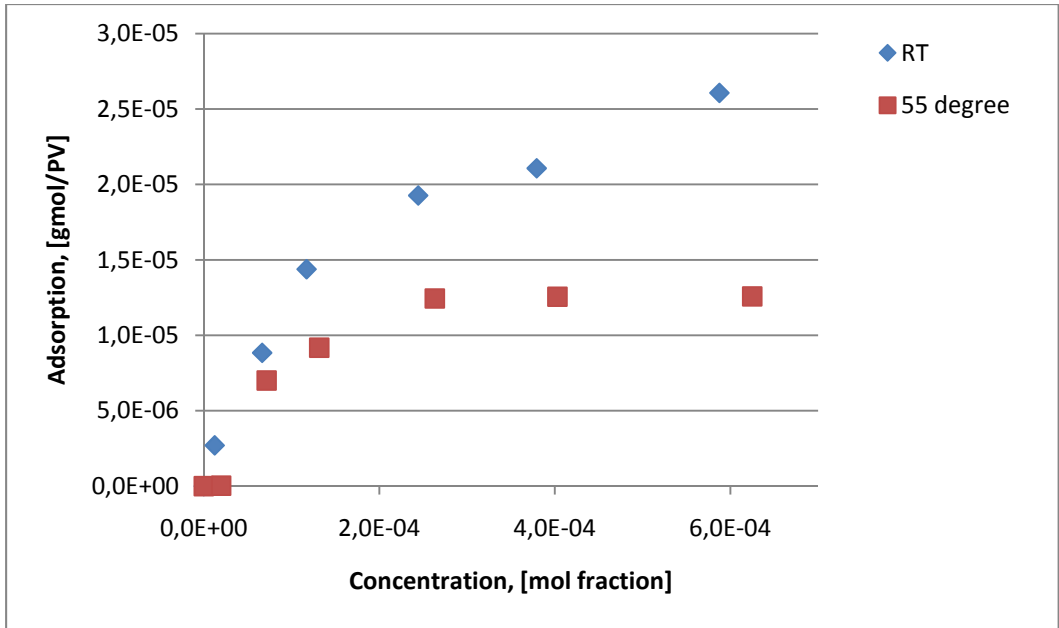


Figure 5.7: Adsorption isotherm in simulation units for the foaming agent from the static experiments at room temperature (RT) and at 55 °C.

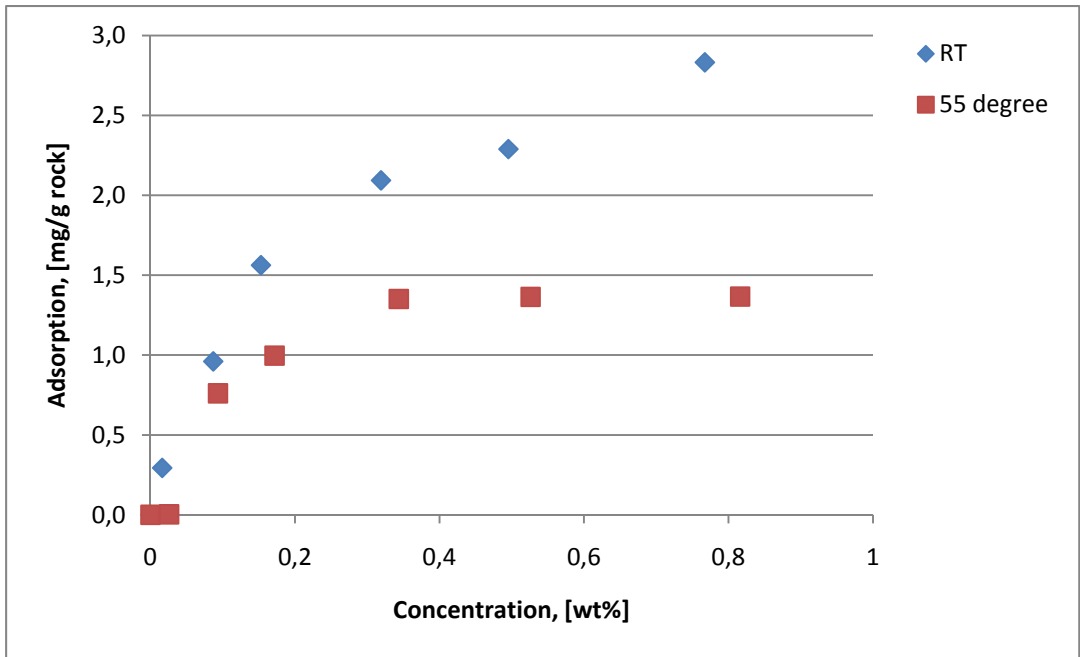


Figure 5.8: Adsorption isotherm in experimental units, at room temperature (RT) and at 55 °C.

It is calculated that the static adsorption of the base case fractured model was 2.31 g/g rock (Table 5.5). The adsorption from the adsorption isotherm in Figure 5.8 is approximately 1.35 mg/g rock at the same concentration. The adsorption is much lower from the static

adsorption experiment, and the reason for this could be that equilibrium was not reached during the experiment. The static adsorption experiment should have been performed over a longer period of time.

5.3 Flow-through retention experiments

The flow-through retention experiment estimates the retention of the foaming agent in a core plug during a dynamical experiment. The adsorption that was found in this experiment could be too low compared to reality, and the static adsorption experiment (section 5.2) could be too high. In the static adsorption experiment it is difficult to find the adsorption for core plugs with S_{or} because many parameters need to be varied; oil, rock, volume of foaming agent solution etc. The flow-through experiments were therefore used to estimate what the adsorption would be for the core plugs with oil. In Figure 5.9 and 5.10 the normalized foaming agent concentration (C/C_0) has been plotted against pore volume (PV). The normalized concentration is the concentration of foaming agent in effluent samples, C , divided on the initial foaming agent concentration, C_0 . The adsorption in the flow-through experiments was found from the difference in area under the lithium graph and the foaming agent graph (Strand et al. 2006).

The flow-through experiments were done with two parallel core plugs at 100 % water saturation, J1 and J3 (Table 5.3), and two parallel core plugs at S_{orw} , D1 and D2 (Table 5.4).

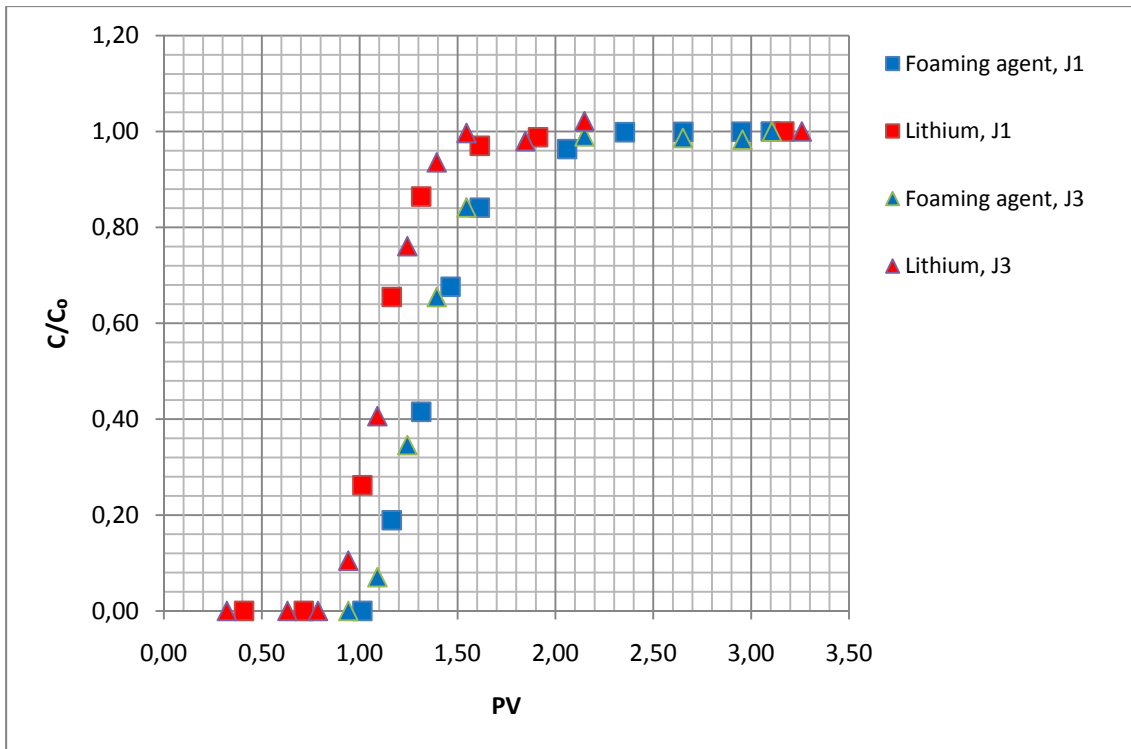


Figure 5.9: Flow-through retention experiment for two parallel core plugs, J1 and J3, at $S_w = 100\%$.

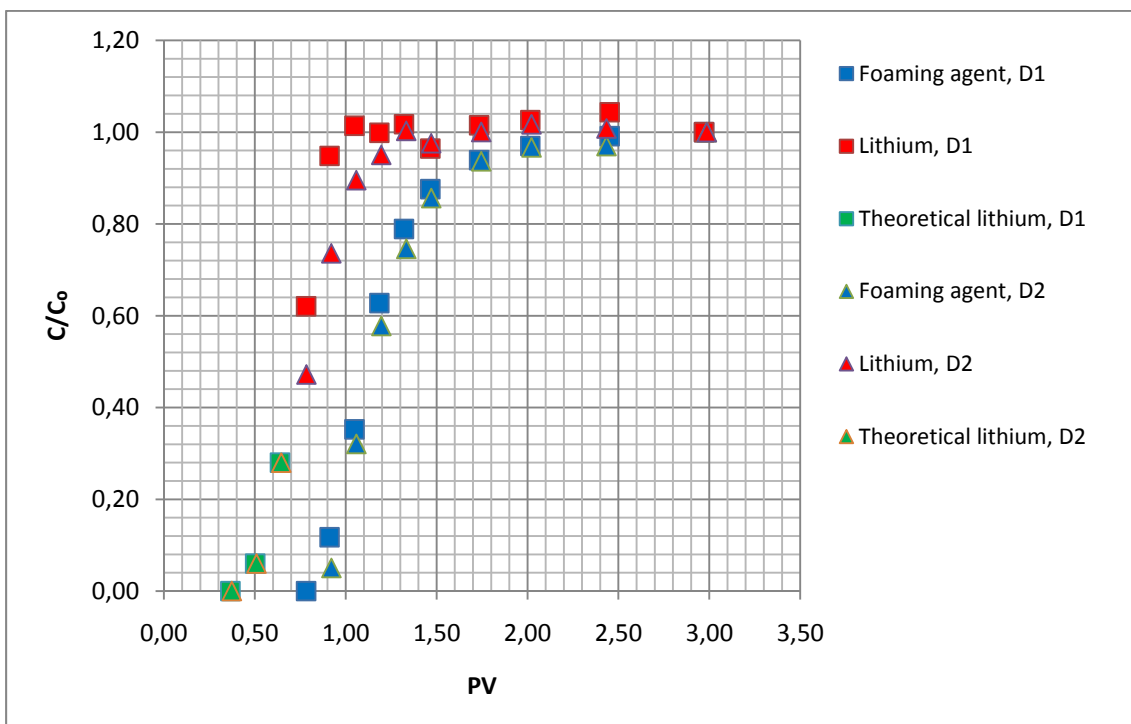


Figure 5.10: Flow-through retention experiment for two parallel core plugs, D1 and D2, at S_{orw} . The lowest three points (green) on the lithium graph are theoretical values of the normalized concentration of lithium determined from the shape of the graphs.

The three lowest points (green points) on the lithium graph for both core plugs D1 and D2 in Figure 5.10 have been estimated by assuming that the shape of the foaming agent graph and the lithium graph should be the same. This was done because the concentration of the selected samples sent to the extern lab were higher than expected, and there was not enough time to send more samples for analysis. These estimated points made it possible to find the area under the lithium graph, and thus the retention by area.

The retention results from the experiment are shown in Table 5.7.

Table 5.7: Retention results from the flow-through retention experiments.

		Retention by area, [mg/g rock]
S_w = 100 %	J1	0.78
	J3	0.95
S_{orw}	D1	1.45
	D2	1.33

In these experiments the core plugs at S_{orw} had a retention that was approximately 0.5 mg/g rock higher than what the retention was for the core plugs at 100 % water saturation (Table 5.7). From the fractured chalk model it was seen that there was almost no difference in the retention at 100 % water saturation and at S_{orw} (Table 5.6). The reason why there was a difference in the flow-through experiments could be because equilibrium had not been reached. To obtain a more correct retention at equilibrium in a dynamic experiment, the experiment should either be performed at a lower rate, or by re-circulation the foaming agent solution.

5.4 Numerical simulation of the fractured model experiment

The experiments were simulated with the reservoir simulator STARS. In STARS the retention of the foaming agent is an important input, and it is described with the adsorption isotherm. In this thesis, the static adsorption experiment (section 5.2) was used to determine the adsorption isotherm of the foaming agent at 55 °C.

In the simulations the objective was to use the parameters from the fractured model experiments, and try to match the experimental results that had been obtained. The simulated results from STARS were plotted together with the results from the experiments, as shown in Figures 5.11 – 5.17.

The base case fractured model where all the surface areas were exposed to the foaming agent solution at 100 % water saturation (Figure 3.4a) was first history-matched. This was done by tuning the diffusion coefficient in the fracture and inside the core plug. The adsorption isotherm found experimentally (section 5.2) was used to describe the adsorption of the foaming agent. When a good match was found, the other designs were predicted using the same data as in the history-matched model. The only parameter that was changed in the predictions was the transmissibility on the surface area that was blocked.

In the two cases where there was an extra core plug at S_{orw} , the experimental results were history-matched. The main differences from these history-matched results and the simulated results at 100 % water saturation were the presence of oil, the effective diffusion coefficient and the maximum adsorption capacity (ADMAXT) in the matrix. The value of S_{orw} was found in Table 5.2. The effective diffusion coefficient at S_{orw} is dependent on both diffusion between foaming agent in water, and foaming agent in oil. Since the diffusion coefficient for foaming agent in oil is not known, the diffusion coefficient will be calculated by multiplying the diffusion coefficient for foaming agent in water with the residual water saturation, $(1 - S_{orw})$. The history-match was done with three different ADMAXT in the matrix. First ADMAXT in the matrix was as experimentally for 100 % water saturation (section 5.2). In addition history-match with ADMAXT in matrix that was 10 times larger and

100 times larger was performed. The reason why a higher ADMAXT in the matrix was tried was because the flow-through experiment showed that the retention was higher at S_{orw} (Table 5.7). The rock and fracture input parameters that were used are shown in Table 5.8.

Table 5.8: Rock and fracture input parameters used in STARS.

Parameter	$S_w = 100\%$	S_{orw}
Maximum adsorption capacity in the matrix, ADMAXT	$1.26 \cdot 10^{-5}$ mol/cm ³ PV	$1.26 \cdot 10^{-b}$ mol/cm ³ PV
Maximum adsorption capacity in the fracture, ADMAXT	0	0
Residual adsorption level, ADRT	0 mol/cm ³ PV	0 mol/cm ³ PV
Accessible pore volume, PORFT	1	1
Residual resistance factor, RRFT	1	1

* b is equal to 5, 4 or 3.

5.4.1 No surface area blocked

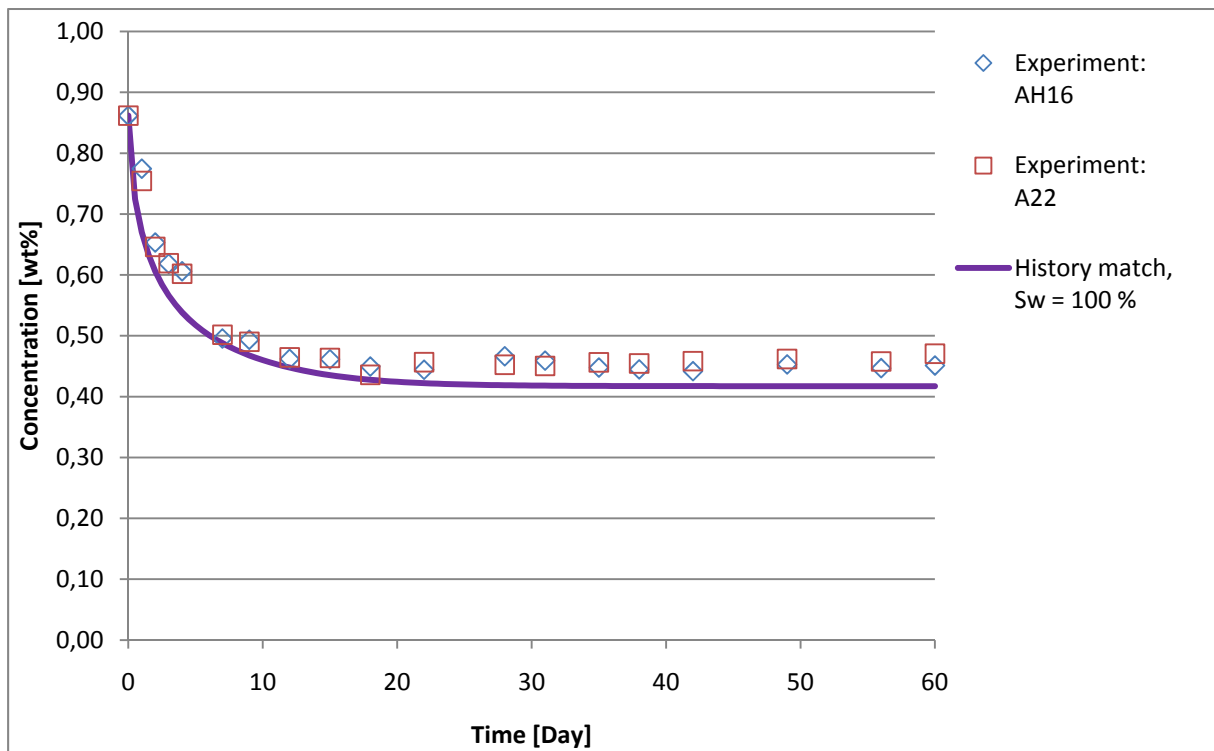


Figure 5.11: Foaming agent concentration vs. time for experiments and history-match where no surface area is blocked and $S_w = 100\%$.

In Figure 5.11 all surface area is exposed to the foaming agent solution and it is at 100 % water saturation. The history-match of the experimental results is presented. This match was achieved by tuning the diffusion coefficient in the core plug and in the artificial fracture. From literature the diffusion coefficient inside the core plug has been found to be in the range of $1 \cdot 10^{-6} \text{ cm}^2/\text{min}$ at room temperature (Rosen 2004). The diffusion coefficient increases with increasing temperature. The best history-match with the experimental results was found when the diffusion coefficient was $3 \cdot 10^{-5} \text{ cm}^2/\text{min}$ inside the core plug. In the fracture the diffusion coefficient selected was several magnitudes larger than the one inside the core plug; $0.01 \text{ cm}^2/\text{min}$. There was a good agreement between the experimental results and the history-match.

5.4.2 Lateral surface area blocked

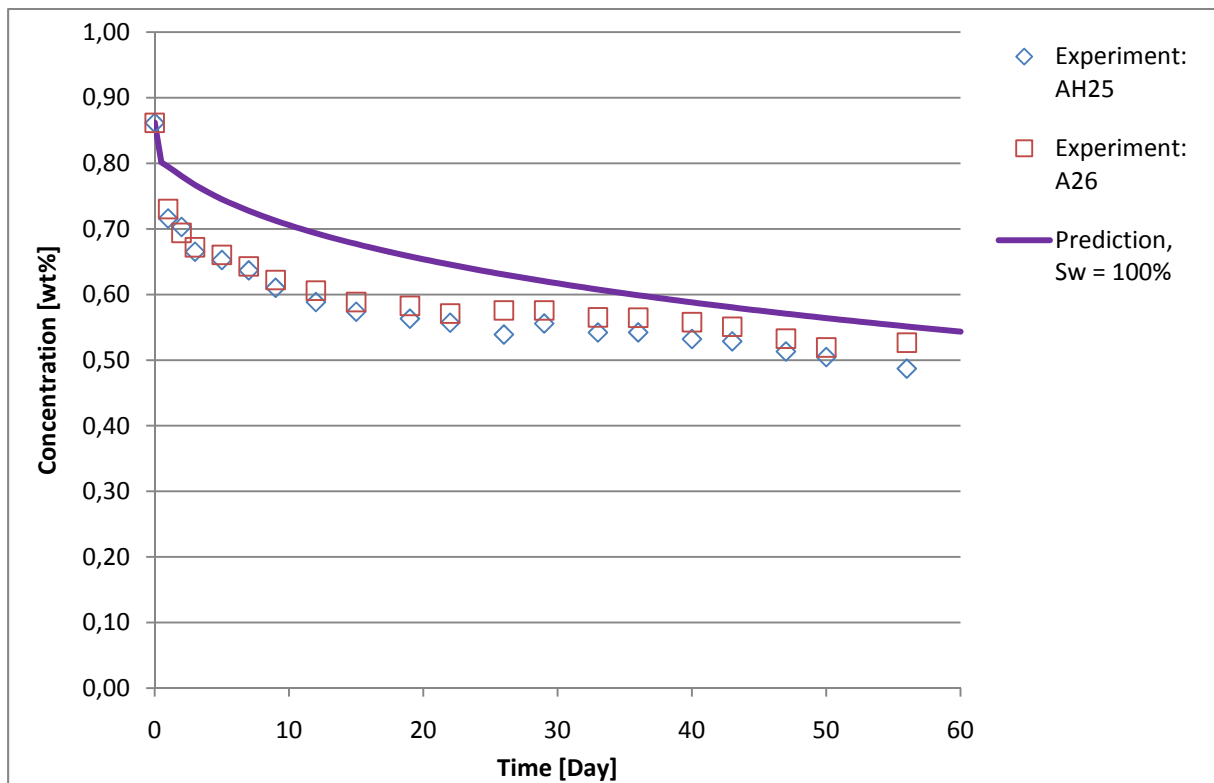


Figure 5.12: Foaming agent concentration vs. time for experiments and prediction where the lateral surface area is blocked, $S_w = 100\%$ for AH25 and A26.

The experimental results and prediction of the design at 100 % water saturation with lateral surface area blocked, i.e. where the foaming agent can be transported through the top and bottom surface area of the core plug, is shown in Figure 5.12. The prediction was approximately 7 – 15 % higher than the experimental results, but the trend of the prediction was similar to the experimental result.

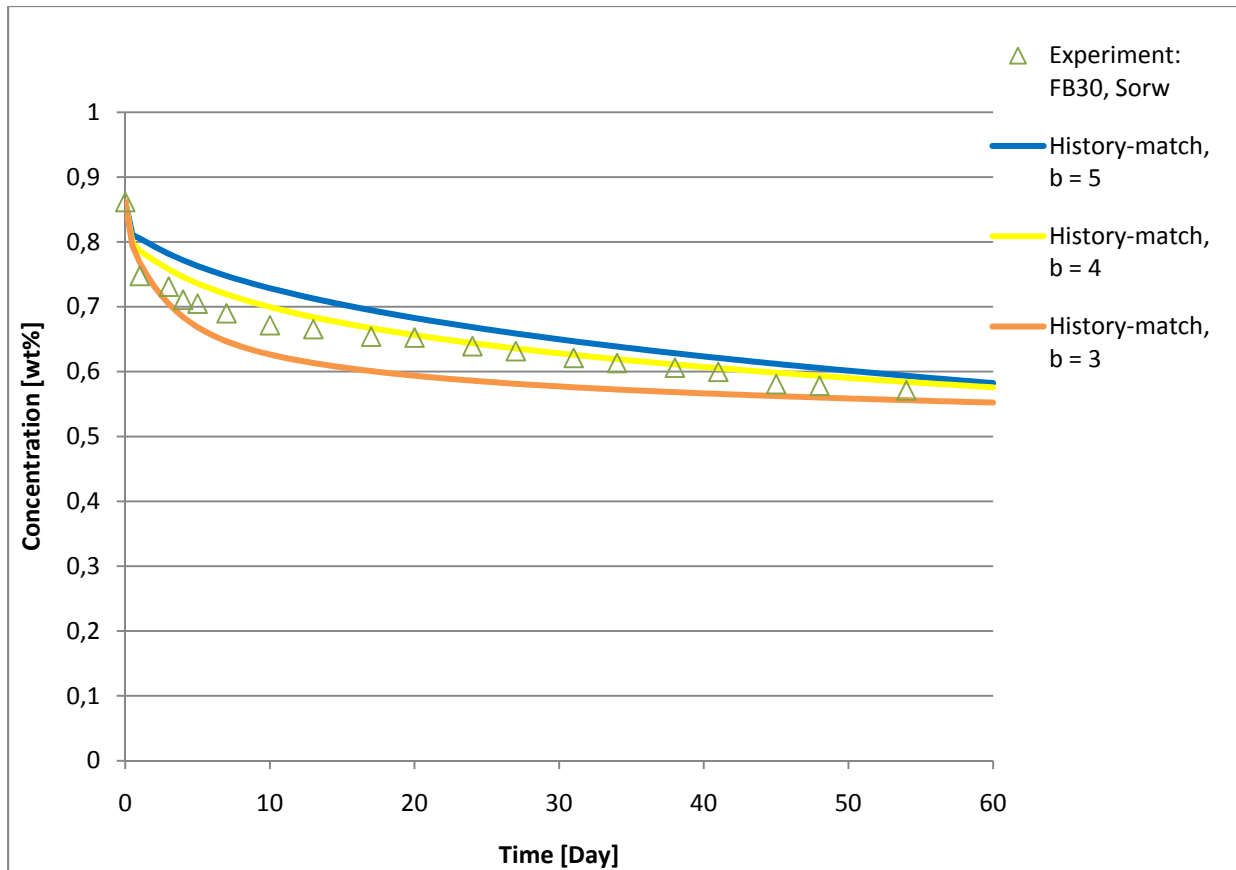


Figure 5.13: Foaming agent concentration vs. time for experiment and different history-matches where the lateral surface area is blocked, FB30 is at S_{orw} . $ADMAXT = 1.26 \cdot 10^{-b} \text{ mol/cm}^3 \text{ PV}$, where $b = 3, 4 \text{ or } 5$.

Figure 5.13 shows the experimental results and different history-matches for the core plug at S_{orw} with the lateral surface area blocked. The S_{orw} for FB30 is approximately 24 % (Table 5.2). The effective diffusion coefficient will therefore be $2.3 \cdot 10^{-5} \text{ cm}^2/\text{min}$ in the core plug. The best history-match for this design was with $b = 4$. This means that the $ADMAXT$ in the matrix was $1.26 \cdot 10^{-4} \text{ mol/cm}^3 \text{ PV}$. This is an adsorption that is 10 times larger than in the cases at 100 % water saturation. This trend of the history-match is similar to the experimental results. The history-match with $b = 5$ and $b = 3$, showed too high and too low foaming agent concentration respectively compared to the experimental results.

5.4.3 Lateral surface area and top blocked

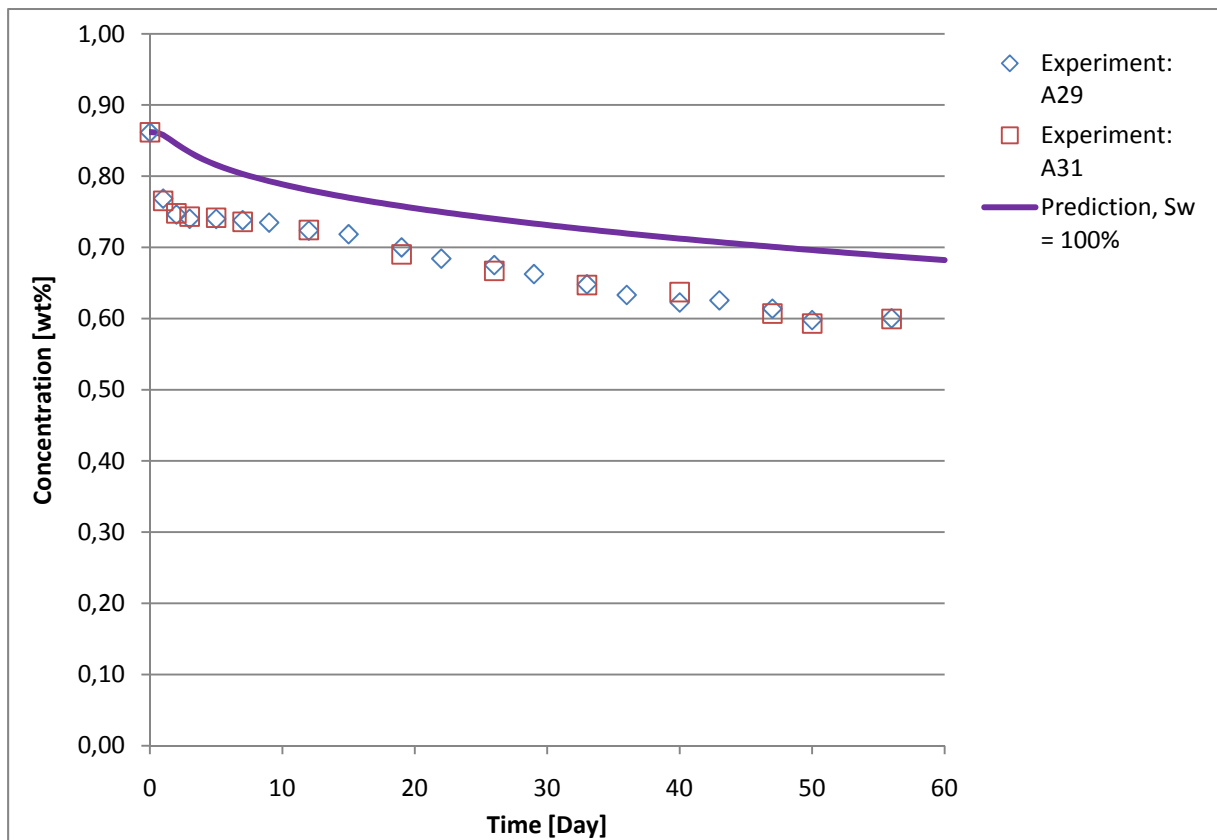


Figure 5.14: Foaming agent concentration vs. time for experiments and prediction where the lateral surface area and top is blocked, at $S_w = 100\%$.

The experimental results and prediction at 100 % water saturation for the design where the only surface area that is open for the foaming agent solution is the bottom of the core plug is shown in Figure 5.14. The predicted result from the simulations showed an approximately 6 – 14 % higher concentration profile than the experimental results showed. The trend of the prediction was similar to the experimental results.

5.4.4 Lateral surface area and bottom blocked

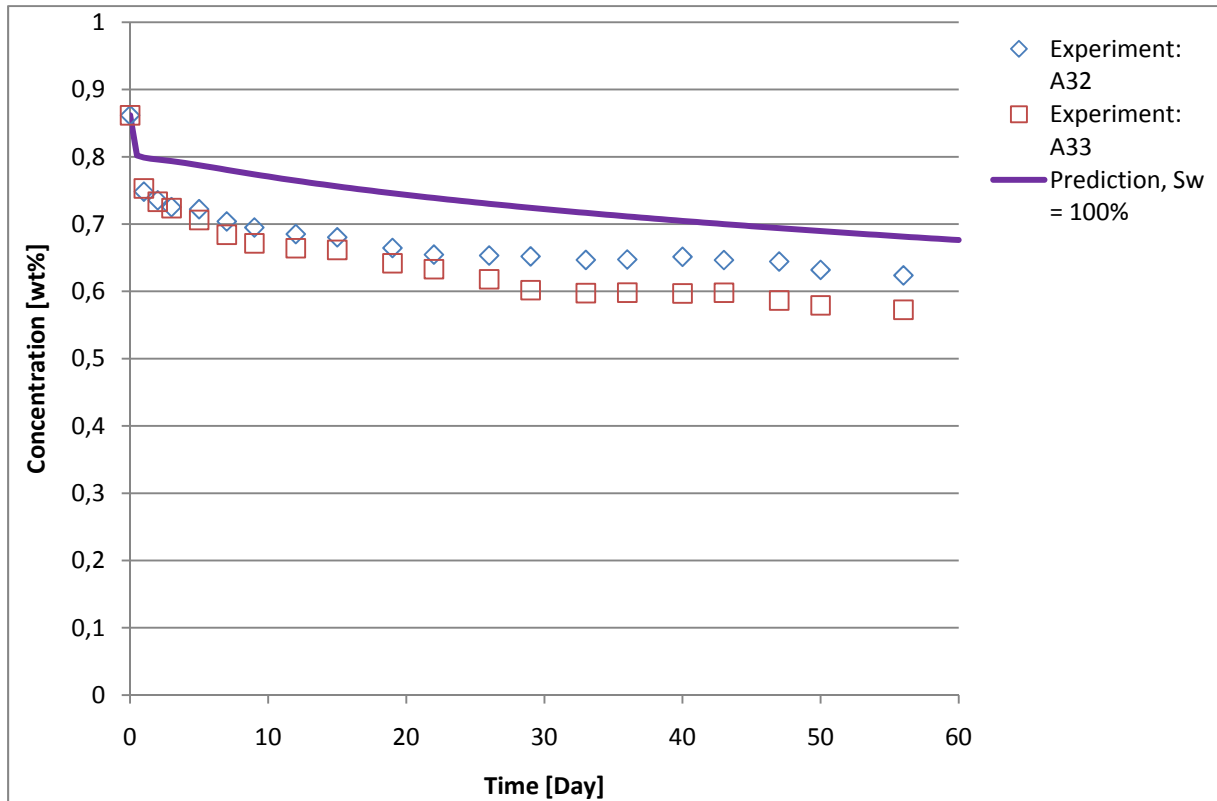


Figure 5.15: Foaming agent concentration vs. time for experiments and prediction where the lateral surface area and bottom is blocked. A32 and A33 is at $S_w = 100\%$.

The prediction of the fractured model with the lateral surface area and bottom blocked at 100 % water saturation together with the experimental results is shown in Figure 5.15. The trend of the prediction was similar to the experimental results. The prediction was approximately 6 – 14 % higher than the results from the experiments.

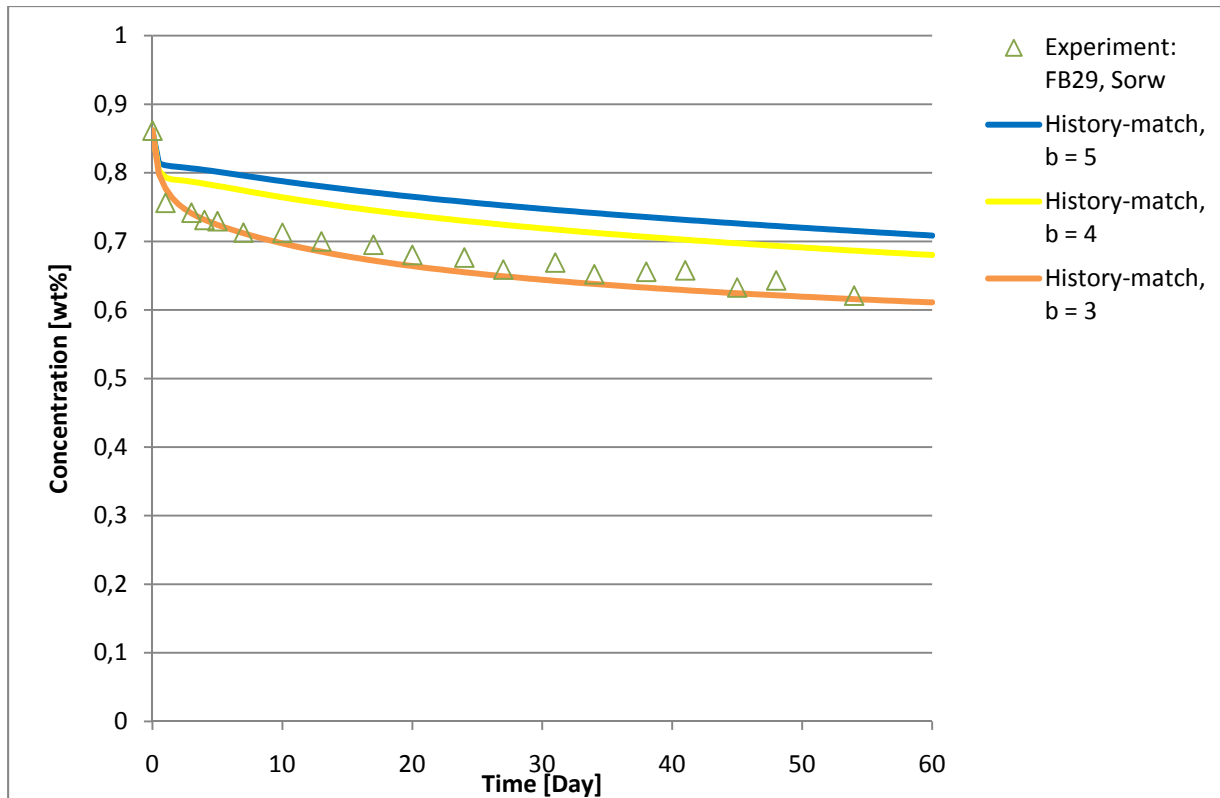


Figure 5.16: Foaming agent concentration vs. time for experiment and different history-matches where the lateral surface area and bottom is blocked, FB 29 is at S_{orw} . $ADMAXT = 1.26 \cdot 10^{-b} \text{ mol/cm}^3 \text{ PV}$, where $b = 3, 4$ or 5 .

Figure 5.16 shows the experimental results and different history-matches for the core plug at S_{orw} with the lateral surface area and bottom blocked. The S_{orw} for FB29 is approximately 30 %. The diffusion coefficient in the core plug will therefore be $2.1 \cdot 10^{-5} \text{ cm}^2/\text{min}$. The best history-match for this design was with $b = 3$. This means that $ADMAXT$ in the matrix was $1.26 \cdot 10^{-3} \text{ mol/cm}^3 \text{ PV}$. This is an adsorption that is 100 times larger than in the cases at 100 % water saturation. The trend of the history-match is similar to the experimental results. The history-match with $b = 5$ and $b = 4$, showed too high foaming agent concentration compared to the experimental result.

5.4.5 Half the lateral surface area and bottom blocked

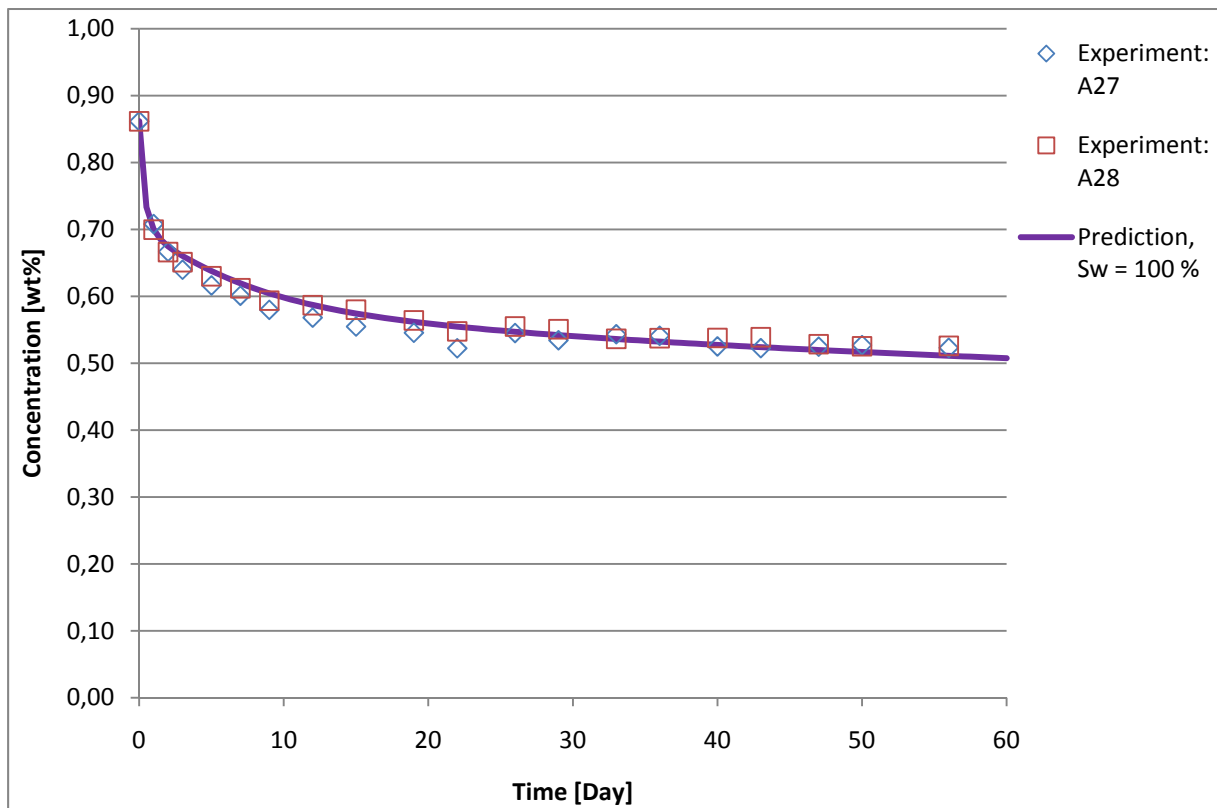


Figure 5.17: Experimental data and simulated data where half the lateral surface area and the bottom are blocked, at $S_w = 100\%$.

The predicted results for the case where half the lateral surface area and bottom is blocked at 100 % water saturation were a very good agreement with the results from the experiments (Figure 5.17). The simulated results followed the experimental results almost perfectly.

5.4.6 Summary of the simulated results

The history-match of the base case at 100 % water saturation was a good match with the experimental results (Figure 5.11). Predictions of the other designs at 100 % water saturation showed different degree of match. The best prediction was the design where half the lateral surface area and the bottom were blocked (Figure 5.17). The other predictions at 100 % water saturation showed foaming agent concentrations that were slightly higher than the experimental results. The reason for the lower concentrations in the experimental results can be because of experimental errors such as concentration determination from the titration, adsorption isotherm could have been too low, or mixing caused by moving the container from the heating oven to the bench for sampling.

There were performed different attempts to history-match the experimental results for the core plugs at S_{orw} . The best match for the core plug with lateral surface area blocked was with ADMAXT equal to $1.26 \cdot 10^{-4}$ mol/cm³ PV (Figure 5.13), and for the core plug with lateral surface area and bottom blocked ADMAXT was $1.26 \cdot 10^{-3}$ mol/cm³ PV (Figure 5.16).

5.5 Simulated results from the core plug with lateral surface area blocked

Some extra simulations were carried out with the lateral surface area blocked at 100 % water saturation. The parameters were the same as the prediction in section 5.4.2. The difference was that it was performed over a longer period of time. This was done to study the distribution of foaming agent across the core plug. The foaming agent that was used in the simulations was the same as used in the experiments in this thesis. The locations on the core plug are shown in Figure 4.2.

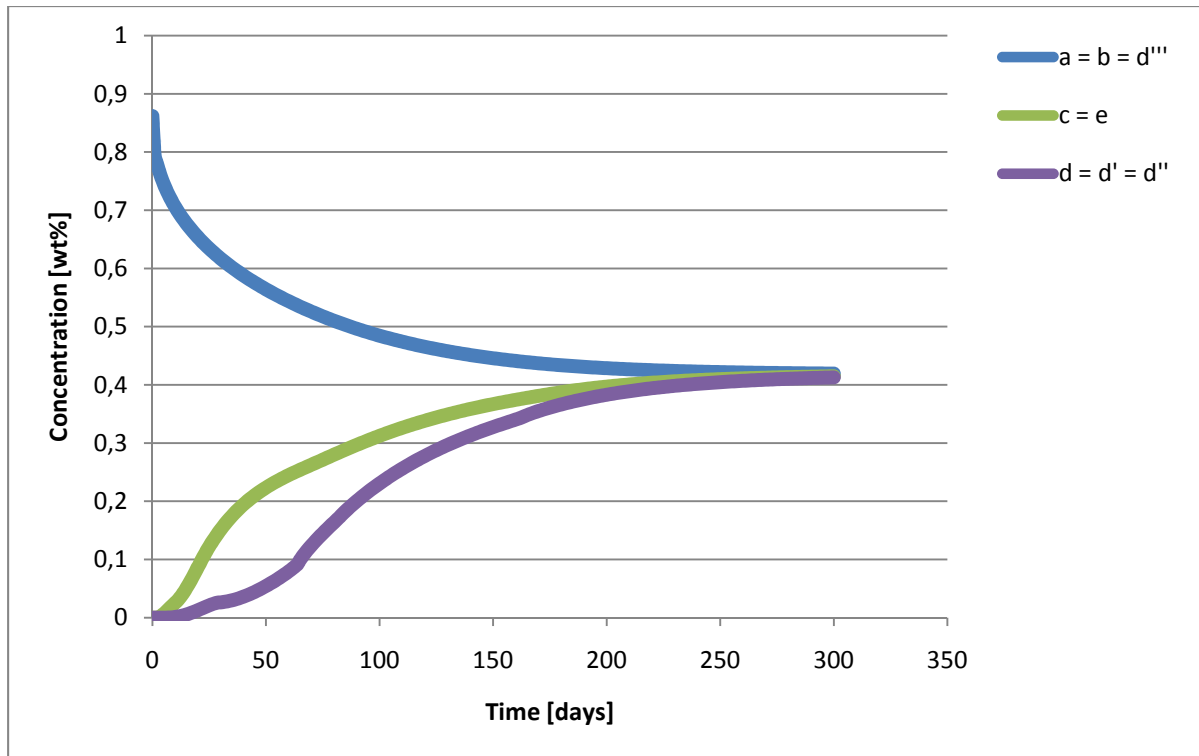


Figure 5.18: Foaming agent concentration vs. time predicted at different locations. The lateral surface area is blocked and $S_w = 100\%$.

Figure 5.18 shows that the equilibrium concentration for this design is reached after approximately 300 days. Some of the foaming agent concentration profiles are approximately the same, and are overlapping each other. As seen in Figure 5.18, the concentration profiles of a, b and d''' are approximately overlapping, c and e are overlapping, and d, d' and d'' are overlapping. The locations a, b and d''' are all in the artificial fracture in the model, and this indicated that there was an almost identical distribution of foaming agent in the fracture. Point c and e are located at the same distance inside the core plug, and this indicated that the foaming agent was transported into the core plug at the same rate from both ends. The points d, d' and d'' showed that the foaming agent in the middle of the core plug was almost evenly distributed. The results also showed that the concentration of the foaming agent decreased toward the middle of the core plug.

5.6 Larger scale simulations

This is the same prediction as in section 5.4.4 at 100 % water saturation, for the same foaming agent. The difference is that it is performed at a larger scale, the length of the core plug was varied, and it was simulated for a longer period of time; 5 000 days. The reason why this design was chosen was because it could be compared with the foaming agent being transported from the fracture and into one side of the matrix block in the reservoir. The simulations were performed to see if the equilibrium concentration would be reached during 5 000 days at a larger scale, and to see how the length of the core plug affected the rate of retention. In Figure 5.19 the change in concentration of the foaming agent in the fracture vs. time is plotted.

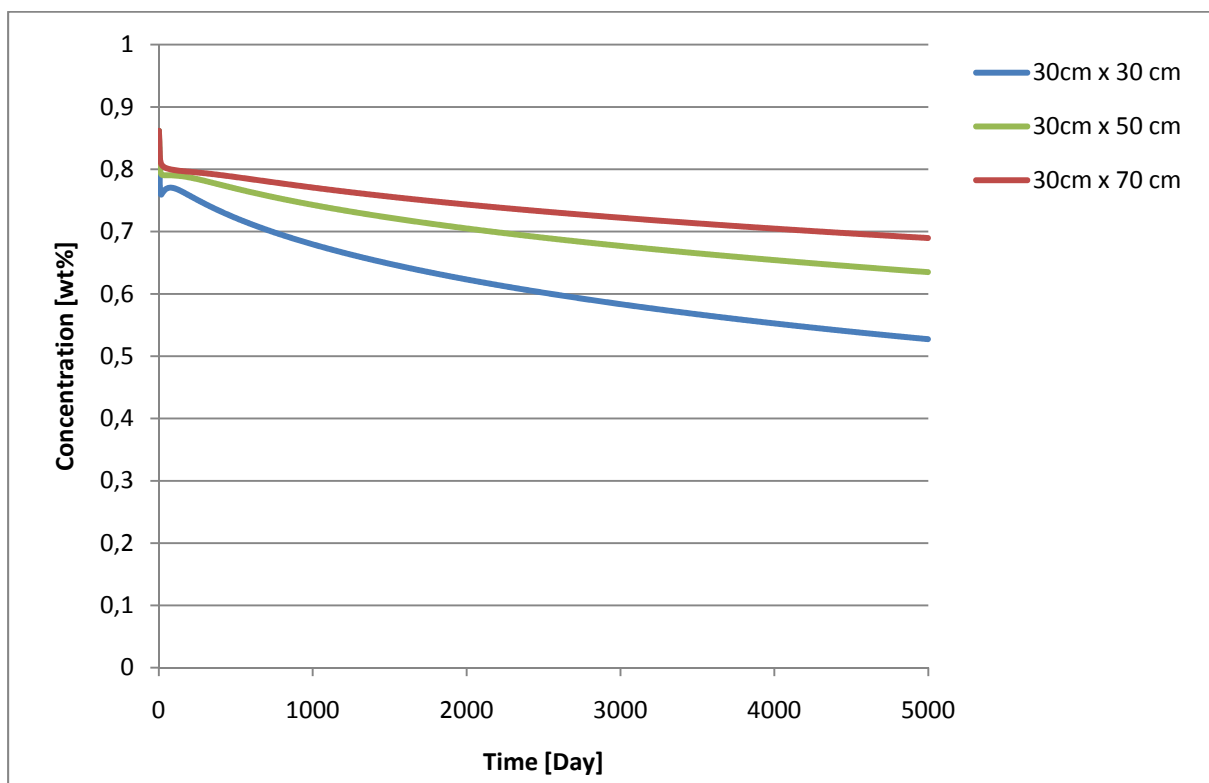


Figure 5.19: Foaming agent concentration vs. time for the prediction of three core plugs with different lengths. The lateral surface and bottom is blocked, and $S_w = 100\%$.

In Figure 5.19 it is seen that all three cases have a fast decline in foaming agent concentration in the fracture during the first days, and then the decline is more slowly. The rate of retention was highest in the core plug with dimensions 30cm x 30cm, and it was lowest in the core plug with dimension 30cm x 70cm. The equilibrium concentration was not reached after 5 000 days. From Figure 5.19 it is seen that the concentration will reach equilibrium first in the case where the core plug is shortest. Earlier performed simulation on large scale with a constant diameter also showed that the transport of foaming agent would depend on the heights of the matrix blocks (Zuta et al. 2010b).

5.7 Comparison

In the base case fractured model the concentration at the end of the experiments was 0.45 wt% and the retention was calculated to be 3.47 mg/g rock after 60 days (Table 5.5). If the concentration of foaming agent is assumed at equilibrium, the static adsorption is calculated to be 2.31 g/g rock. From the static adsorption experiment one could see from Figure 5.8 that if the concentration was 0.45 wt%, the adsorption should be approximately 1.35 mg/g rock. Compared with the calculated static adsorption from the base case in the fractured model, this is a value that is too low. The highest adsorption is expected in the static adsorption experiment because there is a larger accessible area in crushed rock. The reason for the lower adsorption in the static adsorption experiment could be that the equilibrium concentration had not been reached, and it should have been performed over a longer period of time. The average retention from the flow-through experiment at 100 % water saturation was approximately 0.87 g/g rock. This was also a much lower value than the adsorption in the fractured model, and the reason for this might be that equilibrium was not reached.

From the simulated results of the design with the lateral surface area blocked it was seen that the equilibrium concentration was 0.42 wt% and it happened after approximately 300 days (Figure 5.18). In the base case fractured model (section 5.1.1) it is assumed that the

equilibrium concentration is 0.45 wt%. In the determination of the foaming agent concentration there is an uncertainty in the titration of $\pm 5\%$, and this could have caused the difference. Since the concentration of 0.45 wt% is within that uncertainty, it is likely that equilibrium was reached in the base case.

The fractured model showed that the oil saturation had a small affect on the retention of foaming agent (Figure 5.2 and 5.4). The flow-through experiment (section 5.3) showed a higher retention at S_{orw} , the reason for this could be that equilibrium had not been reached.

From the experimental results (Figure 5.1 – 5.5) and simulated results (Figure 5.11 – 5.17) it is seen that the length the foaming agent have to be transported affects the rate of retention and time until equilibrium concentration is reached. This is also seen in the simulations in Figure 5.19. The concentration in the fracture for all the fractured models with different lengths had not reached equilibrium after 5 000 days, which is approximately 14 years. That is a very long time and an EOR process would not be performed over that amount of time. This should be studied further.

6. Discussion

Several studies have been performed on the transport of CO₂-foaming agent during CO₂-foam processes in fractured chalk rock (Zuta et al. 2010b, Zuta and Fjelde 2009). They have shown that time, size of the matrix blocks, concentration of foaming agent solution, chemical structure of foaming agent, temperature, rock type, molecular diffusion, adsorption of the foaming agent, and the presence of oil were important factors that influenced the CO₂-foaming agent transportation from the fractures to the matrix blocks. In the earlier performed experiments all the surface areas on the core plugs have been exposed to the foaming agent solution. The experiments and simulations performed in this thesis showed that the type and amount of surface area of the core plug that was exposed to the foaming agent solution affected the time of foaming agent transport and the amount of retention. The smaller the surface area exposed to the solution, the slower was the transport. The type of surface area blocked affected the time required to reach equilibrium. This was because there was a difference in how far the foaming agent had to be transported to saturate the core plug. If the lateral surface is blocked together with the top or bottom, the solution had a longer way to go to saturate the whole core plug, compared to the core plug with all surface area open.

From the predictions at different locations in the design where the lateral surface area of the core plug was blocked (Figure 5.18), it was seen that the foaming agent concentration inside the core plug decreased towards the center. Zuta and Fjelde (2009) showed this in different experiments.

A limitation in the experiments was that there could have been some mixing in the container when it was moved from the heating cabinet to the bench for sampling. This may have caused faster transport in the fracture. From Figure 5.12, 5.14 and 5.15 it is shown that the

experimental results was lower than the simulated results. The reason could be the extra movement of the container.

Another uncertainty in the experiments was that it was sometimes difficult to find the exact end point during the two-phase titration. The reason for this could be because the different structures in the foaming agent product (IOS) could have slightly different bonding strength to Hyamine. It could also be because the foaming agent solution had a light yellow color, which could have influenced the colors in the titration. This may have caused the results to be slightly higher or lower than it should have been.

When the shrinking-teflon was heated around the core plug, there could have been a change in saturation. The heated air may have caused the water inside the core plug to boil, and thereby change the saturation. This should be investigated further.

The adsorption isotherm that was found in the static adsorption experiment may have been too low compared with the static adsorption calculated in the base case fractured model. The reason for this could be that the equilibrium was not reached during the static adsorption experiment. The adsorption isotherm was used in STARS to simulate the fractured model experimental results. That was because the adsorption results from the fractured model experiments came later. There was not enough time to do the simulations over again with correct adsorption inputs.

From the predictions performed on the design where the lateral surface area was blocked at 100 % water saturation it was seen that equilibrium was reached after approximately 300 days (Figure 5.18). In this case the core plug had a length of 7.0 cm and the foaming agent had the possibility to be transported from both ends of the core plug. Simulations performed in fractured models with varying lengths at larger scale are presented in Figure 5.19. In this case the core plugs had the lateral surface area and bottom blocked at 100 % water saturation. In these cases equilibrium concentration was not reached after 5 000 days. These results may imply that it would take a longer time than the time an EOR process lasts, to saturate the core plug 100 %. This means that most of the foaming agent may be in the

fracture during the process. Upscaling from lab to field should be further investigated in combination with experiments and simulations.

Several parameters were not taken into account during these experiments and simulations because of the time limit. Further work could include:

- Study whether the saturation in the core plug was altered during placement of the shrinking-teflon by heating.
- Repeat the static adsorption experiment over a longer period of time to secure equilibrium.
- Study how the concentration of the foaming agent is distributed inside the core plugs after the retention experiments by drilling out different sections and analyzing these for foaming agent concentration.
- Study how the foaming agent concentration changes vs. time with a core plug that is saturated with oil and all the surfaces are open.
- Vary the transport length by varying the size of the core plugs in fractured models.
- Perform similar experiments with CO₂ present at high pressure.
- Upscaling to a larger scale and perform field scale simulations.

7. Conclusions

Based on the study of foaming agent transport in fractured models of different designs:

- The rate of the foaming agent retention increased with increasing surface area of the core plugs exposed to the foaming agent solution.
- The type of surface area blocked influenced the transport of foaming agent and time it took until the concentration of foaming agent reached equilibrium. The reason for this was that the maximum transport length for the foaming agent varied.
- In all the experiments that were done with core plugs at both 100 % water saturation and at S_{orw} , it was seen that the oil saturation did not have a significant effect on the retention in this thesis.
- A history-match of the base case fractured model at 100 % water saturation was performed, and the predictions of the other fractured model designs at 100 % water saturation were reasonable.
- Predictions performed over a longer period of time on larger scale, showed that it would take a long time until the matrix block was 100 % saturated with the foaming agent.
- The results from the experiments and simulations performed in this thesis may imply that the foaming agent used will have a low retention rate in the field and it may take a long time to saturate the reservoir with the foaming agent.
- Further work with the foaming agent used in this thesis should be performed.

References

- Akbar, M., Vissapragada, B., Alghamdi, A.H., 2000. A Snapshot of Carbonate Reservoir Evaluation. *Oilfield Review* **12** (4): 20-21.
- Apaydin, O.G., and Kovscek, A.R., 2000. Surfactant concentration and end effects on foam flow in porous media. *Transport in Porous Media* **43** (3): 511-536.
- Asghari, K. and Torabi, F., 2008. Effect of Miscible and Immiscible CO₂ flooding on Gravity Drainage: Experimental and simulation results. Paper SPE 110587 presented at the SPE/DOE Improved Oil Recovery Symposium, Oklahoma, USA, 19-23 April.
- Bond, D.C. and Holbrook, O.C., 1958. Gas Drive Oil Recovery Process. U.S. Patent No 2 866 507.
- Casteel, J.F. and Djabbarah, N.F., 1988. Sweep Improvement in CO₂ Flooding by Use of Foaming Agents. SPE 14392. *SPE Res Eng* **3** (4): 1186-1192.
- Chakravarthy, D., Muralidhara, V., Putra, E., Hidayati, D.T. and Schecter, D.S., 2006. Mitigating Oil Bypassed in Fractured Cores During CO₂ Flooding using WAG and Polymer Gel Injections. Paper SPE 97228 presented at the SPE/DOE Symposium on Improved Oil Recovery, Tulsa, Oklahoma, USA, 22-26 April.
- Chang, S.-H., and Grigg, R.B., 1994. Laboratory Flow Tests Used to Determine Reservoir Simulator Foam Parameters for EVGSAU CO₂ Foam Pilot. Paper SPE 27675 presented at the Permian Basin Oil and Gas Recovery Conference, Midland, Texas, USA, 16-18 March.
- Chang, S.-H., and Grigg, R.B., 1999. Effects of Foam Quality and Flow Rate on CO₂-foam Behavior at Reservoir Temperature and Pressure. SPE 56856. *SPE Res Eval & Eng* **2** (3): 248-254.
- Chung, F.T.H., 1991. Modeling Surfactant Transport and Adsorption in Porous Media. Topical report NIPER-510, No.DE-FC22-83FE60149, National Institute for Petroleum and Energy Research (NIPER), Bartlesville Project Office, Bartlesville, Oklahoma, USA, April.
- CMG Manual, Version 2010.10. Computer Modeling Group.
- Darvish, G.R., Lindeberg, E., Holt, T., Utne, S.A. and Kleppe J., 2006. Reservoir-Conditions Laboratory Experiments of CO₂ Injection into Fractured Cores. Paper SPE 99650

- presented at the SPE Europec/EAGE Annual Conference and Exhibition, Vienna, Austria, 12-15 June.
- Dindoruk B. and Firoozabadi A., 1994. Computation of Gas-Liquid Drainage in Fractured Porous Media Recognizing Liquid Flow. Paper CIM-94-23 presented at the 45th Annual Technical Conference of the Petroleum Society of CIM, Calgary, 12-15 June.
- Ettinger, R.A. and Radke, C.J., 1992. Influence of Texture on Steady Foam Flow in Berea Sandstone. SPE 19688. *SPE Reservoir Engineering* **7** (1): 83-90.
- Falls, A.H., Hirasaki, G.J, Patzek, T.W., Gauglitz, D.A., Miller, D.D. and Ratulowski, T., 1988. Development of a Mechanistic Foam Simulator: The Population Balance and Generation by Snap-Off. SPE 14961. *SPE Reservoir Engineering* **3** (3): 884-892.
- Firoozabadi, A. and Markeset, T.I., 1994. Miscible Displacement in Fractured Porous Media: Part I – Experiments. Paper SPE/DOE 27743 presented at the SPE/DOE Symposium on Improved Oil Recovery, Tulsa, Oklahoma, USA, 17-20 April.
- Fjelde, I., 2008. Sulphate in Rock Samples from Carbonate Reservoirs. SCA 2008-19. International Symposium of the Society of Core Analysis, Abu Dhabi, October 29 – 3 November.
- Fjelde, I., Zuta, J. and Duyilemi, O.V., 2008a. Oil Recovery from Matrix during CO₂-Foam Flooding of Fractured Carbonate Oil Reservoirs. Paper SPE 113880 presented at the 2008 SPE Europec/EAGE Annual Conference and Exhibition, Rome, Italy, 9 – 12 June 2008.
- Fjelde, I., Zuta, J. and Hauge, I., 2008b. Retention of CO₂-Foaming Agents on Chalk: Effects of Surfactant Structure, Temperature, and Residual-Oil Saturation. Paper 113259 presented at the SPE/DOE Symposium on Improved Oil Recovery, Tulsa, 20 – 23 April 2008.
- Green, D.W., and Willhite, G.P., 1998. *Enhanced oil recovery*. Richardson, Texas, USA: SPE textbook series, volume 6.
- Grigg, R.B. and Mikhalin, A.A., 2007. Effects of Flow Conditions and Surfactant Availability on Adsorption. Paper SPE 106205 presented at International Symposium on Oilfield Chemistry, Houston, Texas, USA, 28. February- 4. March.
- Hardman, R.F.P., 1982. Chalk Reservoirs of the North Sea. *Bull. Geol. Soc. Denmark*, **30**: 119-137.
- Hirasaki, G.J. and Lawson, J.B., 1985. Mechanisms of Foam Flow in Porous Media: Apparent Viscosity in Smooth Capillaries. *SPE Journal* **25** (2): 176-190. SPE 12129.

- Holm, L.W. and Josendal, V.A., 1974. Mechanisms of Oil Displacement by Carbon Dioxide. *Journal of Petroleum Technology* **26** (12): 1427-1438. SPE 4736.
- Hoteit, H. and Firoozabadi, A., 2006. Numerical Modeling of Diffusion in Fractured Media for Gas Injection and Recycling Schemes. Paper SPE 103292 presented at the SPE Annual Technical Conference and Exhibition, San Antonio, Texas, USA, 24-27 September.
- Kovscek, A.R., Patzek, T.W. and Radke, C.J., 1993. Simulation of Foam Transport in Porous Media. Paper SPE 26402 presented at the Annual Technical Conference and Exhibition, Houston, Texas, USA, 3-6 October.
- Kovscek, A.R. and Radke, C.J., 1994. Fundamentals of Foam Transport in Porous Media. In *Foams: Fundamentals and Applications in the Petroleum Industry*; ed L.L. Schramm; Washington, D.C., USA; Advances in Chemistry; American Chemical Society. **242**: 115-163.
- Kovscek, A.R., Trethewey, D., Persoff, P. and Radke, C.J., 1995. Foam Flow through a Transparent Rough-Walled Rock Fracture. *Journal of Petroleum Science and Engineering* **13** (2): 75-86. NETL 1244.
- Kuehne, D.L., Frazier, R.H., Cantor, J. and Horn, W., 1992. Evaluation of Surfactants for CO₂ Mobility Control in Dolomite Reservoirs. Paper SPE 24177 presented at the 1992 SPE/DOE Symposium on Enhanced Oil Recovery, Tulsa, Oklahoma, USA, 22-24 April.
- Latil, M., 1980. *Enhanced Oil Recovery*. Ed. Technip, Paris. Institut Français du Pétrole Publications.
- Lee, H.O., Heller, J.P. and Hoefler, A.M.W., 1991. Change in Apparent Viscosity of CO₂-foam with Rock Permeability. *SPE Reservoir Engineering* **6** (4): 421-428. SPE 20194.
- Mannhardt, K. and Novosad, J.J., 1994. Adsorption of Foam-Forming Surfactants for Hydrocarbon-Miscible Flooding at High Salinities. In *Foams: Fundamentals and applications in the petroleum Industry*, ed L.L. Schramm, Chap. 7, 259-318. Washington, DC, USA: Advances in Chemistry Series; American Chemical Society.
- Merck, KGaA. 2003. Sulfate Cell Test, Spectroquant 1.14548.0001, E.91145.4892/07-6000274017 msp. 01/03.
- Nguyen, Q.P., Alexandrov, A.V., Zitha, P.L. and Currie, P.K., 2000. Experimental and Modeling Studies on Foam in Porous Media: A Preview. Paper SPE 58799 presented at the SPE

- International Symposium on Formation Damage Control, Lafayette, Louisiana, USA, 23-24 February.
- Orr, F.M., Heller, J.P. and Taber, J.J., 1982. Carbon Dioxide Flooding for Enhanced Oil Recovery: Promise and Problems. *Journal of American Oil Chemists Society* **59** (10): 810A-817A.
- Panahi, H., 2004. Improving the Recovery Factor of Heavy Crude Reservoirs by Co-injection CO₂ and Other Conventional Gaseous Injecting Materials at Immiscibility Conditions with Foam. Paper SPE 92011 presented at the SPE International Petroleum Conference in Mexico, Puebla Pue., Mexico, 7-9 November.
- Rosen, M.J., 2004. Surfactants and Interfacial Phenomena, Third Edition. John Wiley & Sons, Inc.
- Scamehorn, J. F., Schechter, R.S. and Wade, W.H., 1982. Adsorption of Surfactants on Mineral Oxide Surfaces from Aqueous Solutions; I: Isomerically Pure Anionic Surfactants; *Journal of Colloid and Interface Science* **85** (2).
- Schmitt, T.M., 1992. Titration of Surfactants. In *Analysis of Surfactants*. Surfactant science series, volume 40. Chap. 11, 344-348. Marcel Dekker, Inc. New York, USA.
- Schramm, L.L. and Wassmuth, F., 1994. Foams: Basic Principles. In *Foams: Fundamentals & Applications in the Petroleum Industry*, ed. L.L. Schramm, Chap. 1, 3-46. Washington, DC, USA: Advances in Chemistry Series, American Chemical Society.
- Shan, D. and Rossen, W.R., 2002. Optimal Injection Strategies for Foam IOR. Paper SPE 75180 presented at the SPE/DOE Improved Oil Recovery Symposium, Tulsa, Oklahoma, USA, 13-17 April.
- Somasundaran, P. and Fuerstenau, D.W., 1966. Mechanisms of Alkyl Sulfonate Adsorption at the Alumina-Water Interface. *Journal of Physical Chemistry* **70**: 90.
- Strand, S., Standnes, D.C., and Austad, T., 2006. New Wettability Test for Chalk based on Chromatographic Separation of SCN⁻ and SO₄²⁻. *J. Pet. Sci. Eng.* **52** (1-4): 187-197.
- Strand, S., Hjuler, M.L., Torsvik, R., Madland, M.V. and Austad, T., 2007. Wettability of Chalk: Impact of Silica, Clay Content and Mechanical Properties. *Petroleum Geosciences*, **13** (1): 69-80.
- Tabatabal, A., Gonzalez, M.V., Harwell, J.H. and Scamehorn, J.F., 1993. Reducing Surfactant Adsorption in Carbonate Reservoirs. *SPE Res Eng* **8** (2): 117-122. SPE 24105.

- Yan, W., Miller, A., Hirasaki, G.J., 2006. Foam Sweep in Fractures for Enhanced Oil Recovery. *Colloids and Surfaces A: Physicochemical Engineering Aspects* 282-283: 348-359.
- Zuta, J. and Fjelde, I., 2009. Transport of CO₂-foaming agents during CO₂-Foam Processes in a Fractured Chalk Rock. Paper SPE 121253 presented at the SPE EUROPEC/EAGE Annual Conference and Exhibition, Amsterdam, The Netherlands, 8-11 June.
- Zuta, J., Fjelde, I., and Berenblyum, R., 2010a. Experimental and Simulation of CO₂-Foam Flooding in Fractured Chalk Rock at Reservoir Conditions: Effect of Mode of Injection on Oil Recovery. Paper SPE 129575 presented at the SPE EOR Conference at Oil & Gas West Asia, Muscat, Oman, 11-13 April.
- Zuta, J., Fjelde, I., Berenblyum, R., Vartdal, L. H. and Ovesen, H., 2010b. Modeling of Transport of a CO₂-Foaming agent during CO₂-Foam Processes in Fractured Chalk Rock. Paper SPE 129601 presented at the SPE Improved Oil Recovery Symposium, Tulsa, Oklahoma, USA, 24-28 April.